


Research Article

The paleoenvironment and depositional context of the Sumerian site of Abu Tbeirah (Nasiriyah, southern Mesopotamia, Iraq)

Luca Forti^{a,b}, Licia Romano^c, Alessandra Celant^d, Franco D'Agostino^c, Federico Di Rita^d, Jaafar Jotheri^e, Donatella Magri^d, Ilaria Mazzini^f, Daniel Tentori^f and Salvatore Milli^{f,g*} 

^aDipartimento di Scienze della Terra “Ardito Desio”, Università di Milano, Milano, Italy; ^bIstituto di Geoscienze e Georisorse, Consiglio Nazionale delle Ricerche, Pisa, Italy; ^cDipartimento “Istituto Italiano di Studi Orientali, SAPIENZA Università di Roma, Roma, Italy; ^dDipartimento di Biologia Ambientale, SAPIENZA Università di Roma, Roma, Italy; ^eDepartment of Archaeology, University of Al-Qadisiyah, Diwaniyah, 88, Iraq; ^fIstituto di Geologia Ambientale e Geoingegneria, Consiglio Nazionale delle Ricerche, Roma, Italy and ^gDipartimento di Scienze della Terra, SAPIENZA Università di Roma, Roma, Italy

Abstract

The Sumerian culture flourished within the Tigris and Euphrates rivers floodplains and along their deltaic systems, which ca. 6000 yr were located ~250–260 km inland from the present Persian Gulf. Here, large floodplains and marshes were crossed by an intricate network of channels where several human settlements developed. In this paper, we describe in detail the paleoenvironmental context where the site of Abu Tbeirah (third millennium BC) developed, near the Sumerian capital of Ur. Our interdisciplinary approach, based on remote sensing and the geomorphological study of the area, as well as on sedimentological, paleontological, and paleobotanical analyses of trenches and boreholes deposits, reveals that the site developed along a sinuous channel in a floodplain and marshy environment, where several crevasse splays occurred. This channel was cut off following a flood event. The abandoned portion of the channel was exploited by residents and used as a small river harbor. Our research contributes to better define how the landscape of the site changed over the course of its history and how humans exploited water resources of the area during occupation of the site, a process that was pivotal for the development of the Sumerian culture.

Keywords: Mesopotamian plain, Sumerian, Holocene, paleoenvironmental reconstruction, Abu Tbeirah site

(Received 15 July 2021; accepted 9 April 2022)

INTRODUCTION

The Mesopotamian plain occupies the central and southern sector of the Iraq territory and consists of an extensive, low-relief floodplain occupied by the two main rivers (Tigris and Euphrates) and their tributaries (Fig. 1). Since the beginning of archaeological research in the area (Woolley, 1962; Adams, 1965, 1981), the close connection between ancient Mesopotamian cities and the hydrology of the Tigris and Euphrates fluvial systems during the last 6000 yr has been recognized as a pivotal factor for the evolution of the Sumerian society. In particular, the surveys of the last century detected and jointly mapped settlements and water resources (also by using remote sensing techniques) and led researchers to hypothesize a close connection between fluvial dynamics of the Euphrates and Tigris rivers with their tributaries, and the abandonment or reorganization of settlement patterns (Adams, 1965, 1981; Wilkinson, 2001; Pournelle, 2003, 2007; Morozova, 2005; Algaze, 2008; Di Giacomo and Scardozzi, 2012; Jotheri, 2018; Jotheri et al., 2018; Altaweel et al., 2019; Hammer, 2019; Jotheri and Allen, 2020). The resulting depositional context,

characterized by floodplains and marshes crossed by an intricate system of natural and artificial channels, was often utilized as waterways for agricultural irrigation and secondarily for fishing and transport. These waterways have been recognized in different archaeological sites of the southern Mesopotamia (Verhoeven, 1998; Steinkeller, 2001; Pournelle, 2003; Morozova, 2005; Kennet and Kennet, 2006; Heyvaert and Baeteman, 2008; Wilkinson et al., 2015; Jotheri et al., 2016; Pournelle et al., 2019; Engel and Brückner, 2021). Most of the largest cities, such as Ur, Uruk, Eridu, and Girsu, probably developed in relation to precise water management and exploitation of the natural and artificial channels that would contribute to the growth of cities, agriculture, and intercity transport systems (Algaze, 2008; Wilkinson et al., 2015; Hritz and Pournelle, 2016; Schrakamp, 2018) (Fig. 1B).

The purpose of this article is to describe the local landscape evolution of the Abu Tbeirah site, framing it in the context of the paleogeographic evolution of the Persian Gulf at the transition between the Middle and Late Holocene (see Holocene subdivision on International Chronostratigraphic Chart v.2022/02, <https://stratigraphy.org/ICSChart/ChronostratChart2022-02.pdf>). The use of different approaches for analysis of the site (geomorphological, sedimentological, paleontological, paleobotanical, and remote sensing) allowed us to produce a detailed paleoenvironmental

*Corresponding author e-mail: <salvatore.milli@uniroma1.it>

Cite this article: Forti L et al (2022). The paleoenvironment and depositional context of the Sumerian site of Abu Tbeirah (Nasiriyah, southern Mesopotamia, Iraq). *Quaternary Research* 110, 165–183. <https://doi.org/10.1017/qua.2022.22>

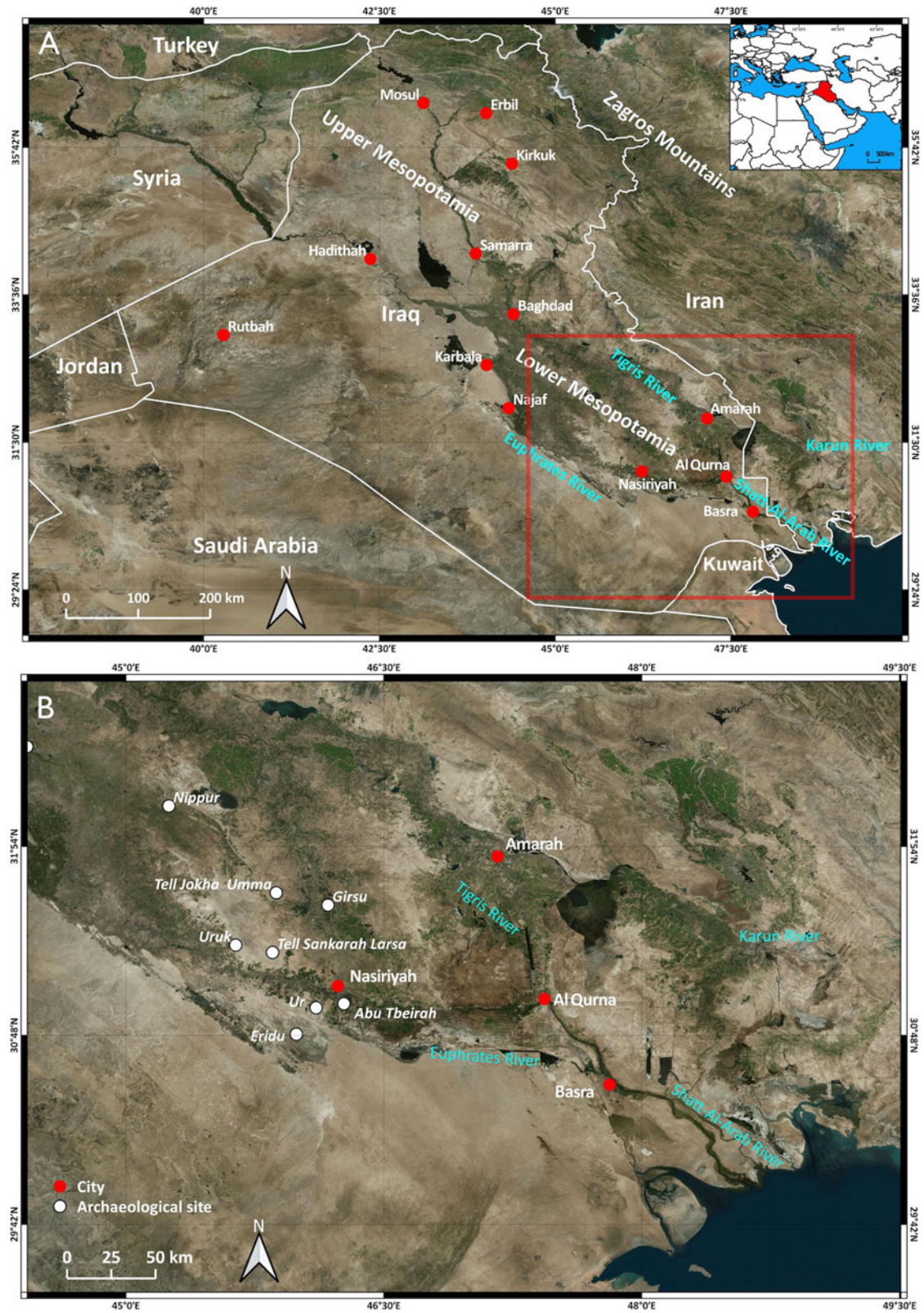


Figure 1. (A) Geographic map of Iraq; the red square indicates Figure 1B; (B) detail showing the main archaeological sites occurring in the Abu Tbeirah surrounding area (modified from Microsoft Bing Maps Virtual Earth).

reconstruction that, together with the archaeological survey carried out over the last years, has provided further details on how the Sumerians exploited the freshwater to brackish fluvial-marshy

environment of the Abu Tbeirah site and how they may have used and managed water resources during settlement life of the third millennium BC.

GEOLOGICAL AND GEOMORPHOLOGICAL SETTING

Mesopotamia and the Persian Gulf constitute a subsiding peripheral foreland basin located between the Arabian plate and the south-west migrating Zagros fold-and-thrust-belt (ZFTB) (Alavi, 2007) (Fig. 2). This basin developed during the late Cenozoic as a consequence of the collisional and post-collisional phases of the Arabia and Eurasia plates (Dercourt et al., 1986; Alavi, 2004; Agard et al., 2005; Jassim and Goff, 2006; Navabpour and Barrier, 2012; Pirouz et al., 2015, 2017).

Subsurface investigations of the Mesopotamian plain have shown the presence of several buried tectonic elements, including folds, faults, and diapiric structures. Many of these buried structures are still active, indicating neotectonic movement that can be observed through their effects on the Pleistocene–Holocene stratigraphy and coastline position, and through modification of Quaternary landforms (Baltzer and Purser, 1990; Al-Sakini, 1993; Al-Kadhimi et al., 1996; Sissakian, 2000; Fouad and Sissakian, 2011; Sissakian and Fouad, 2012; Fouad, 2012; Sissakian et al., 2020).

Quaternary deposits cover the entire lower Mesopotamian plain (LMP) and derive from erosion of the Zagros fold-and-thrust belt and the Arabian Platform. They are essentially represented by alluvial deposits of the Tigris and Euphrates rivers and their tributaries, although the final infill of

the basin is also characterized by aeolian, lacustrine, marshy, and deltaic/estuarine deposits (Yacoub et al., 1985; Aqrabi and Evans, 1994; Yacoub, 2011).

The archaeological site of Abu Tbeirah developed within the Holocene deposits (15–20 m thick). They can be subdivided into three stratigraphic units (from bottom to top): (1) a lower fluvial sandy unit, rich in gypcretes, often associated to ancient playa deposits; (2) an estuarine brackish/marine unit; and (3) an upper fluvial/lacustrine unit (Yacoub et al., 1985; Aqrabi, 1995a, b; Yacoub, 2011). Units 1 and 2 are transgressive and were deposited during the Holocene sea-level rise (Early and early Middle Holocene), whereas unit 3 was formed during the Holocene highstand phase (late Middle and Late Holocene) and shows a progradational trend.

At present, the middle part of LMP is characterized by a landscape with a wide floodplain, including active fluvial channels, natural levees, crevasse splays, and flood basins that are inundated by the water of the Tigris and Euphrates rivers during the spring floods (Fig. 3). This area also displays desert environments (western sector) with dune fields and deflation areas that are subject to intensive salinization (Aqrabi and Evans, 1994; Verhoeven, 1998; Morozova, 2005). The most depressed sector of this area is covered by shallow fresh-/brackish-water lakes, surrounded by reed beds and marshes (Ahwar) where

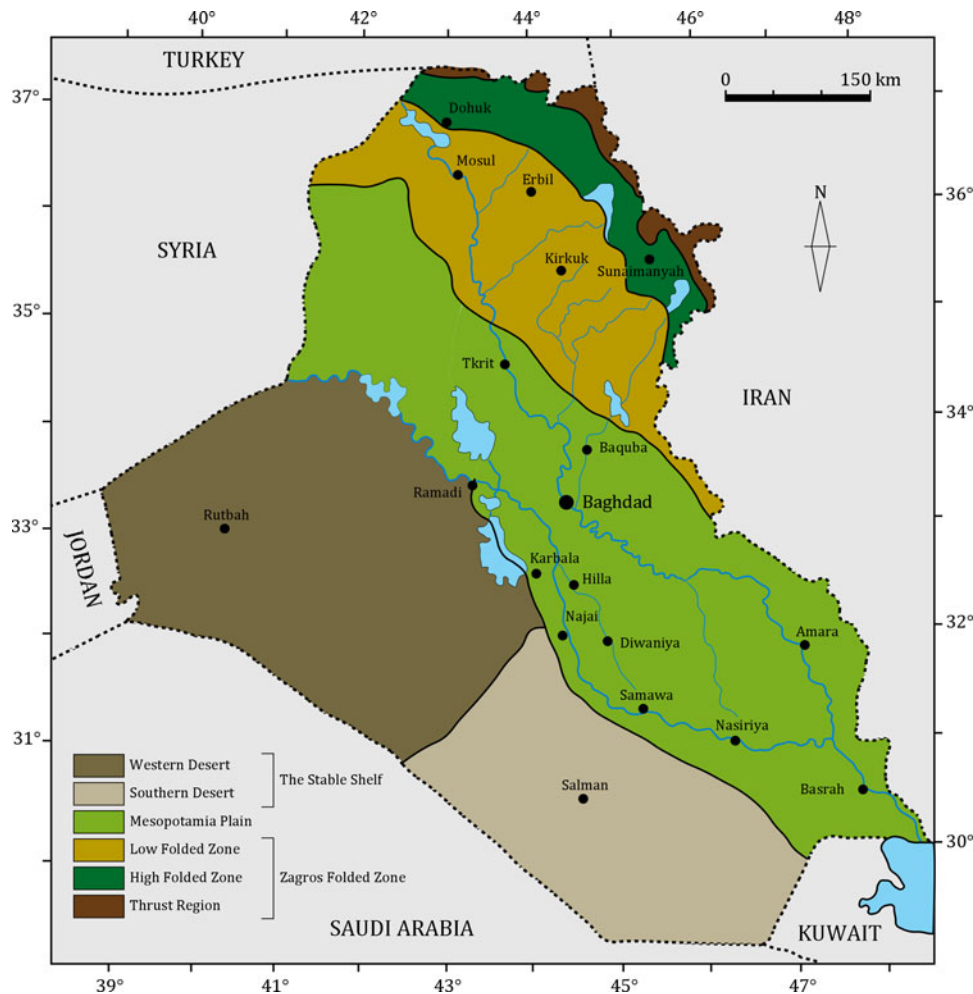


Figure 2. Simplified geological map showing the main tectonic zone in Iraq (modified after Fouad, 2012; Sissakian, 2013).

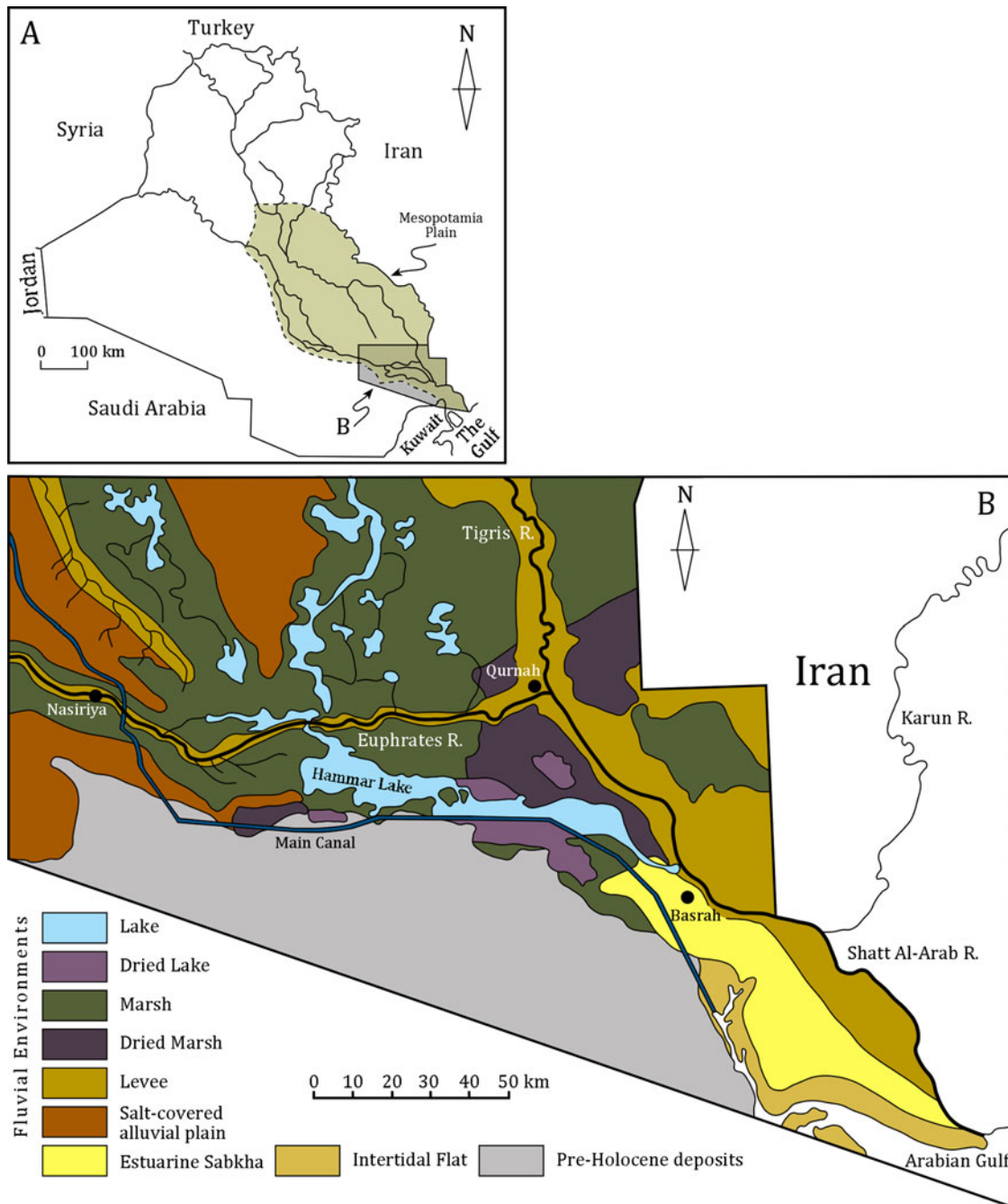


Figure 3. (A) Physiographic map of Iraq showing the location of the Mesopotamian Plain and the detail of the study area. (B) Enlarged map showing the lakes and marshes (Ahwar) occurring in the study area. Modified from Aqrabi and Evans (1994).

the most extensive brackish-water lake (called the Hammer Lake) occurs.

As highlighted by more recent studies using a combination of geological, geomorphological, remote sensing, historical, and archaeological approaches (Hritz and Wilkinson, 2006; Jotheri et al., 2016, 2018), the present drainage pattern of the plain is rather different from previous patterns over the last 6000 years, with this setting reflecting neotectonic movements, fluvial processes, and human activities (Heyvaert and Baeteman, 2008; Heyvaert et al., 2012; Wilkinson et al., 2015). Consequently, most of the archaeological studies that have been carried out in this area (e.g., Adams, 1981; Cole, 1994; Cole and Gasche, 1998;

Morozova, 2005) have assumed that periods of active channels are closely linked to the age of archaeological settlements and that most of the identified ancient settlements were established on the sectors where active channels occurred (Adams, 1981; Wilkinson et al., 2015; Jotheri et al., 2016; 2018).

ARCHAEOLOGICAL SETTING

The Abu Tbeirah site is located 7 km south of Nasiriya and is divided in four sectors by traces of an ancient channel running northwest to southeast, and by a modern north-south oriented pipeline (Fig. 4). The site covers an area of ~42 ha. The

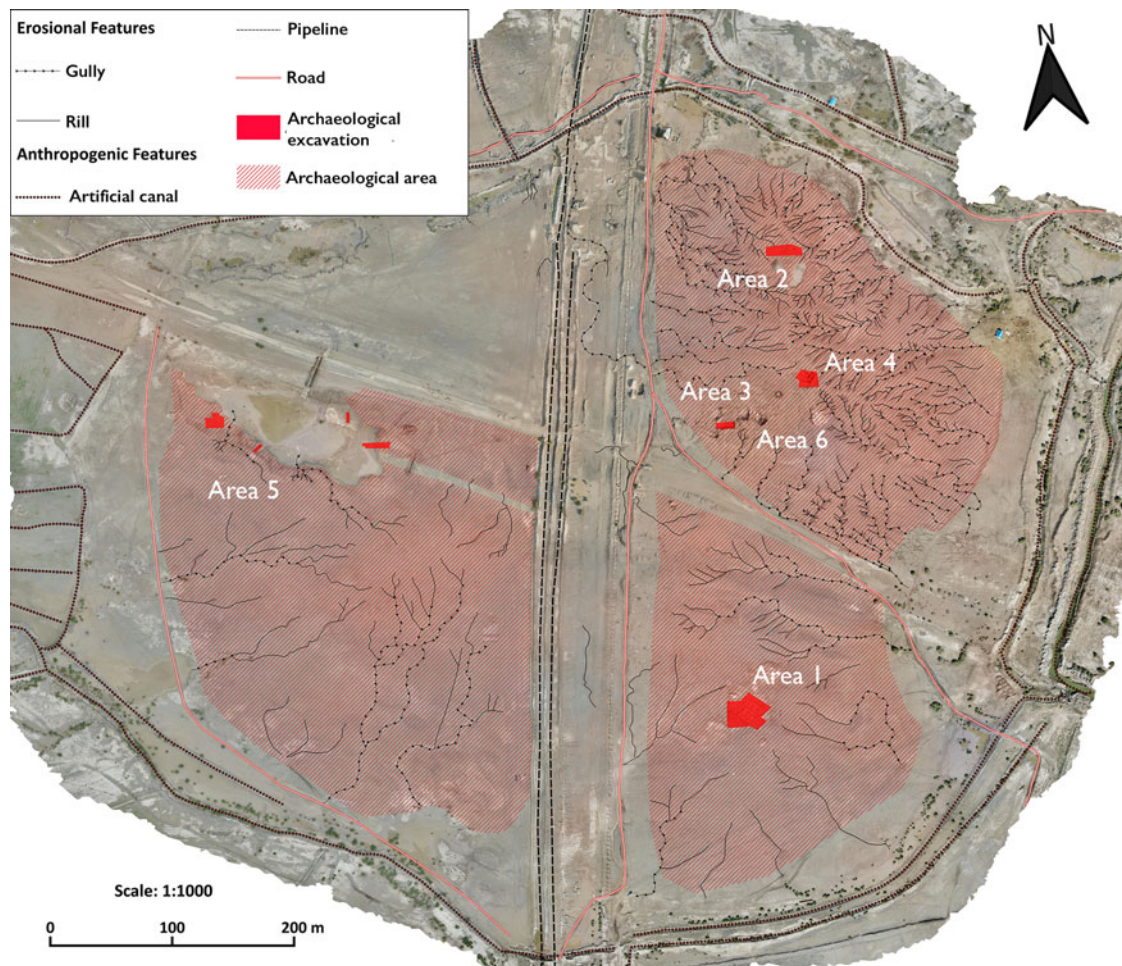


Figure 4. UAV orthophoto of Abu Tbeirah site and the surrounding area showing the main geomorphological elements, anthropogenic features, and archaeological areas with the excavated sectors.

northwestern sector of the tell has suffered the heaviest damage. Across almost the entire extent there are modern large and deep pits and corresponding heaps of unearthed soil.

The northeastern sector is the highest portion of the site (elevation of 4 m amsl) reaching a maximum height of 4.30 m with respect to the surrounding area (Areas 2, 3, 4, and 6; Fig. 4). On the surface, pottery and other materials are not particularly abundant, except for the northeastern portion of the mound (Area 2) where archaeological materials were brought to the surface by modern activities, and by deep gullies eroded by rainfall. Sporadic findings, both from the surface and the excavation of the northeastern and southeastern areas, revealed possible occupation since the Uruk-Jemdet Nasr Period. In particular, Area 6 shows an occupation lasting until at least the reign of Amar-Suena, based on two half-bricks discovered in the foundation of a building (D'Agostino and Romano, 2020a, b). Areas 2 and 4 present other apparently domestic buildings, although constructed with bigger walls than those of Area 1 (southeast sector) (D'Agostino and Romano, 2020a). At present, the artifacts recovered in this part of the tell, except for Area 6 Ur III pottery, do not show substantial differences with the third millennium (plausibly Early Dynastic-Akkadian transition) assemblages in Area 1, although it is possible to tentatively assign this context to a later chronology on the basis of few changes in the pottery repertoire.

In the southeastern sector, Area 1 investigations (Fig. 4) involved surface clearing of $\sim 1000 \text{ m}^2$, revealing the presence of a large articulated complex of buildings that seem to form a unit and that, given the size, might have played a specific role in the life of the settlement.

In Area 5 (southwestern sector), a more depressed area occurs that is interpreted as a small harbor. Near the basin, a dense settlement is easily recognizable, rising alongside what appears to be a wide, straight SE-NW oriented road. Based on the few materials recovered on this part of the tell, a date to the end of the third millennium BC is hypothesized.

Summing up, Abu Tbeirah was a medium-sized city of the third millennium BC. The site mainly flourished during the Early Dynastic period (2900–2350 BC), after which the settlement gradually contracted towards the northeastern sector of the site in which evidence of a limited Ur III and early Old-Babylonian occupation recently was discovered (early second millennium BC). However, it must be stressed that our periodization can be affected by the strong erosion and salinization of the tell surface. At present, it is not possible to determine how much of the site has been eroded. Moreover, the low amount of artifact dispersion on the surface can hide a chronological span wider than that detected at this stage.

General considerations about the ancient urban layout of Abu Tbeirah derive from the analysis of satellite imagery. The

topographic characteristics of the tell show the presence of ancient fluvial channels, around which the settlement was organized. Moreover, satellite imagery allowed us to identify different mud-bricks structures, revealed on the surface by the dark traces left by the buried walls (D'Agostino and Romano, 2020a, b).

Further excavations and studies will still be needed to have a clearer chronological correlation among the Abu Tbeirah areas.

MATERIALS AND METHODS

In addition to archaeological excavations carried out in recent years, the landscapes of the site and the surrounding areas were preliminarily examined through remote sensing analysis. Sedimentological, compositional, paleontological, and paleobotanical analyses were carried out from three trenches (trench Gamma and Delta excavated in 2018 and trench Mal in 2019) and three boreholes (BHA, BHH, BHB; 18, 6, and 5 m deep, respectively) (Fig. 5) in order to define the paleoenvironmental context of the site. The positions of the trenches and boreholes were chosen based on previous archaeological excavations in order to construct a correlation panel that would highlight the stratigraphic and facies relationships among the investigated deposits.

Remote sensing data were provided from several available datasets. High-resolution (0.5–1 m) satellite images, derived from Microsoft Bing Maps Virtual Earth and historical declassified Corona images taken in 1967 and 1968 (DS1039-2088DF073; DS1103-1041DA062; <https://corona.cast.uark.edu>), were visualized and compared in QGIS software to recognize landscape changes. More details were derived from the addition of an AW3D30 Digital Surface Model (DSM) with 1° horizontal resolution (~30 m at the equator) available on the Japan Aerospace Exploration Agency (JAXA, 2020) platform, which was reprojected and resampled to UTM Zone 38N with 30-m spatial resolution. An elevation-dependent color scale was applied to the Digital Surface Model in order to observe small- to large-scale landforms and to recognize the ancient fluvial pattern, as well as the crevasse splays and archaeological sites (e.g., Iacobucci

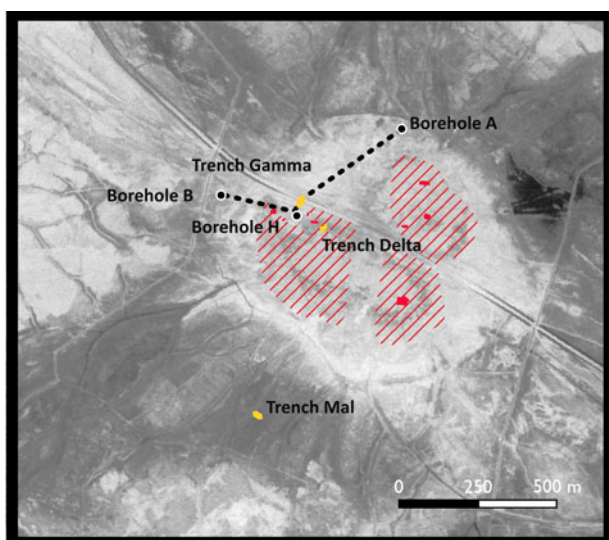


Figure 5. Declassified Corona satellite image showing the locations of the boreholes (BHA, BHH, BHB) and excavated trenches Gamma, Delta, and Mal. The dotted line indicates the track of the correlation panel (Fig. 15).

et al., 2020; Jotheri and Allen, 2020). To confirm and validate the geomorphological elements detected from satellite imagery, several field surveys were carried out over the last few years to ground-truth the remote sensing results and avoid any misinterpretation.

For the archaeological site mapping, UAV imagery was acquired during several archaeological missions and used to create a detailed geomorphological and geoarchaeological map of the tell. Afterwards, the photos were uploaded into Agisoft Metashape photogrammetry software to process the orthophotos, which were then imported and further processed in QGIS software.

Sedimentological analysis included facies definition through grain-size analysis and other textural attributes, as well as sedimentary structures, paleocurrents, and color of the deposits. Other features, such as the presence of shelly debris, clasts of clay, organic matter, wood fragments, and roots, also were taken into consideration for paleoenvironmental interpretation. Stratigraphy of the trenches and boreholes was also utilized to better define, at local and large scales, geometries of the sedimentary bodies and the facies relationships.

To investigate the textural and compositional characters of these deposits, nine samples from trench Gamma and one sample from archaeological Area 1 were sieved to define their grain-size distribution. Additionally, quantitative petrographic analysis of two representative sand samples (125–500 μ) from trench Gamma and the archaeological area, was conducted to compare their compositional characters with those of other samples from Tigris, Euphrates, and Mesopotamia floodplain deposits. The thin sections of sand samples were stained with alizarine red to distinguish calcite and dolomite. Sand composition was quantified using the Gazzi-Dickinson point-count method (Ingersoll et al., 1984). Counted grains were grouped into monomineralic and polymineralic categories, including the metamorphic rock classification by Garzanti and Vezzoli (2003). For sand classification, we used the descriptive nomenclature based on QFL (quartz, feldspar, lithic) proportions as proposed by Garzanti (2019), as well as the LmLvLs (metamorphic lithic, volcanic lithic, sedimentary lithic) proportions for the provenance analysis.

Paleontological analysis was conducted on 12 samples (8 samples from BHA, 2 samples from BHH, and 2 samples from trench Gamma), in which ostracods and malacofauna were found. All sediment samples were soaked in a 5% H₂O₂ solution for 24–48 h, washed on 0.063 mm mesh sieve, and dried. Ostracod adult valves were hand-picked under the stereomicroscope and counted. Ostracod taxonomical identification followed Meisch (2000) and Karanovic (2012). The taxonomical identification of the mollusk shells makes it possible to reconstitute biocenotic assemblages and thus to identify the conditions that prevailed during development of these species (biotopes). Shells and shell fragments were collected after wet sieving using 2 mm, 1 mm, and 0.5 mm mesh sieves. Mollusk taxonomical identification and palaeoecology followed Plaziat and Younis (2005).

Paleobotanical analysis was carried out on pollen (4 samples from BHH, and 2 samples from BHA) and on plant macroremains (5 samples from BHH). For pollen analysis, samples were chemically treated following a standard procedure with HCl (37%), HF (40%), and NaOH (10%) (Magri and Di Rita, 2015). Pollen concentrations were determined by adding a known number of *Lycopodium* spores to known weights of sediment. Pollen grains were identified by means of a light microscope at $\times 400$ and $\times 630$ magnifications. At least two slides per

Table 1. Radiocarbon dates from cores and trench of the Abu Tbeirah site.

Sample	Type	Lab. Code	$\delta^{13}\text{C}$ ‰	Conventional ^{14}C yr BP	Calibrated ^{14}C yr BP	Status
BHA (439–464 cm)	mud	LTL19059A	-27.5 ± 0.5	11872 ± 80	14012–3514	rejected
BHA (860–871 cm)	mud	LTL19060A	-26.7 ± 0.5	7839 ± 250	9404–8179	rejected
BHA (1531–1539 cm)	sandy sediment	LTL19061A	246.2 ± 0.6	32684 ± 250	37703–6324	rejected
BHH (500–510 cm)	mud	LTL19062A	-34.3 ± 0.7	12332 ± 75	14844–4078	rejected
Trench Delta (100–120 cm)	organic sediment	LTL19063A	-23.1 ± 0.4	3980 ± 45	4572–4292	accepted

sample were analyzed. Plant macro-remain analysis was carried out on 5 samples consisting of fragments of unburnt vegetable fiber—essentially reeds. These remains were water-separated from a known weight of sediment (~50 g per sample) and analyzed by means of a stereomicroscope.

Five samples from borehole BHA (3), BHH (1), and trench Delta (1) were selected for AMS radiocarbon dating and were sent to the Dating and Diagnostic Center (CEDAD) of Salento University (Italy) (Table 1). Calibration of radiocarbon dates was based on the IntCal20 datasets (Reimer et al., 2020) by means of the Calibration Program Calib 8.20 (Stuiver and Reimer, 1993). Unfortunately, only the sample from trench Delta was useful for dating the deposits because the other samples showed contamination by circulating carbon, rendering their ages inconsistent with the archaeological data.

RESULTS

Present landscape and remote sensing data

The present landscape of Abu Tbeirah and the surrounding area is influenced by fluvial processes of the Euphrates and is characterized by a wide floodplain with both active and ancient watercourses (Fig. 3). Remote sensing analysis revealed several crevasse splays and flood basins that are active during intense precipitation and during periods of high discharge in the Euphrates

and its tributary channels. Comparison between the 1967 declassified Corona images and the current UAV orthophotos reveals an increase of anthropic activity due to the expansion of the city of Nasiriyah, excavation of canals, and intense land use, together with the presence of natural small-scale erosional features such as gullies and rills (Fig. 4). Abu Tbeirah was strongly affected by post-depositional processes, and several anthropogenic features were mapped, including deep trenches and related embankments of a pipeline crossing the site from north to south (Fig. 4). Moreover, one artificial basin and canals were excavated around the site to drain and collect water after intense precipitation due to the complex local drainage system of gullies and rills.

Remote sensing analysis allowed us to identify 36 archaeological mounds in the surrounding Abu Tbeirah region, including the sites previously surveyed near Ur (Fig. 6) (see also Adams, 1981; Jotheri, 2019). These sites differ in size, but all the sites are smaller than Ur. Abu Tbeirah, which is the second largest site after Ur, has a location and alignment consistent with the identified paleochannels.

Only two paleochannels were clearly identified in the surveyed area (Fig. 6): the larger one is associated with Ur; the other one is associated with Abu Tbeirah. Based on the sedimentological analysis conducted in this study, the courses of this latter channel were partially modified in the past.

Near the studied site, remote sensing analysis enables identification of at least eight crevasse splays connected to the initial

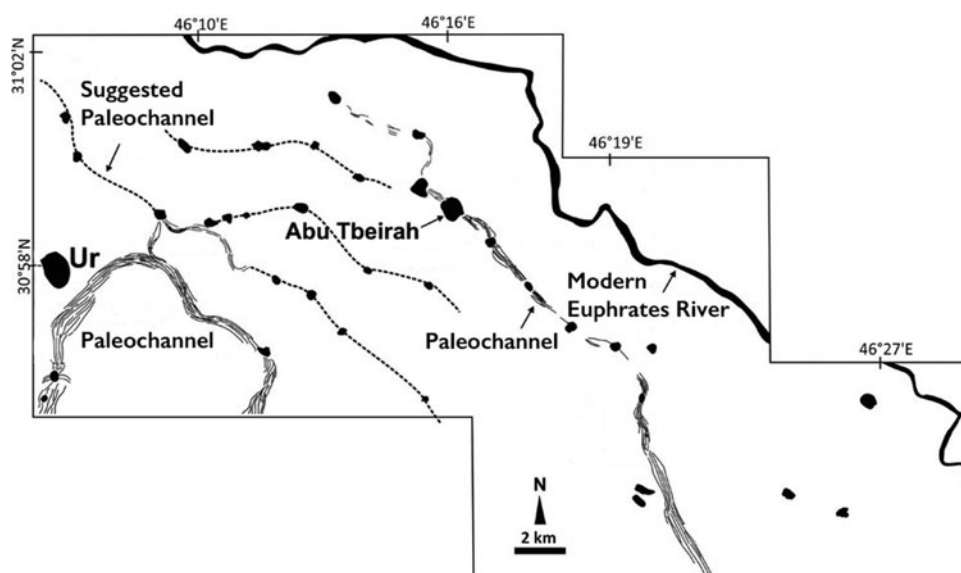


Figure 6. Suggested and reconstructed paleochannels in the area surrounding the Abu Tbeirah site (modified from Jotheri, 2019). Archaeological sites are in black.

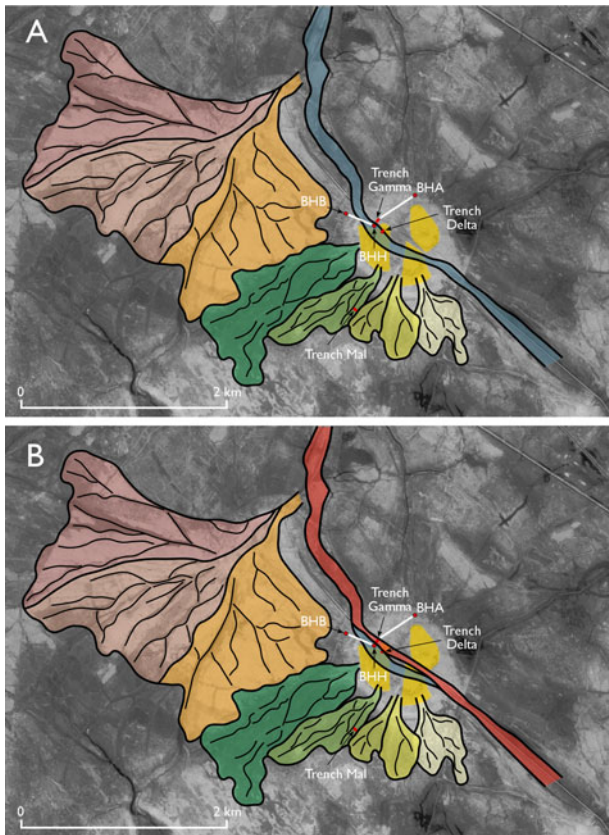


Figure 7. (A) Reconstructed plan geometry of the Abu Tbeirah area on declassified Corona satellite image showing the presence of crevasse splay related to the activity of the initial sinuous channel (in blue) before the chute cut-off. Note the decreased dimensions of the crevasse splays moving from NW to SE. (B) Reconstructed direction of the new Abu Tbeirah channel (in red) after the chute cut off. The two solid white lines indicate the track of the correlation panel shown in Figure 15; archaeological areas are in yellow.

sinuous Abu Tbeirah channel, having variable dip and strike dimensions from 2000–570 m and from 850–180 m, respectively (Fig. 7A). The crevasse splays show a convex-up profile along dip at the proximal sector that gradually flattens floodplain-ward. Along strike, the profile tends to vary depending on the activity of the channels crevasse. Each strike-section at the proximal, middle, and distal sectors shows a flattening and decrease in thickness of the bodies towards the floodplain. As visible in Figure 7, the dimensions of these crevasse splays decrease from NW to SE and form two composite bodies that we argue are strictly correlated to the evolutive phases of the initial sinuous Abu Tbeirah channel. The proximal sector of these crevasse splays shows structureless fine and very fine sand beds (20–50 cm thick) constituting the filling of shallow channels. The latter pass transitionally downstream to middle and distal sectors that are dominated by lobe deposits. Here, finer and thinner cross-laminated sand beds with load structures occur and pass farther down current to structureless silt deposits, and finally to the flood-basin mud (see also Bridge and Demicco, 2008; Burns et al., 2017; Gulliford et al., 2017). Such deposition reflects flow deceleration, passing from confined to unconfined conditions (i.e., from distributive crevasse channels in the proximal sector to lobe deposits in the middle and distal sectors; see also Yuill et al., 2016; Van Toorenburg et al., 2018).

Compositional data

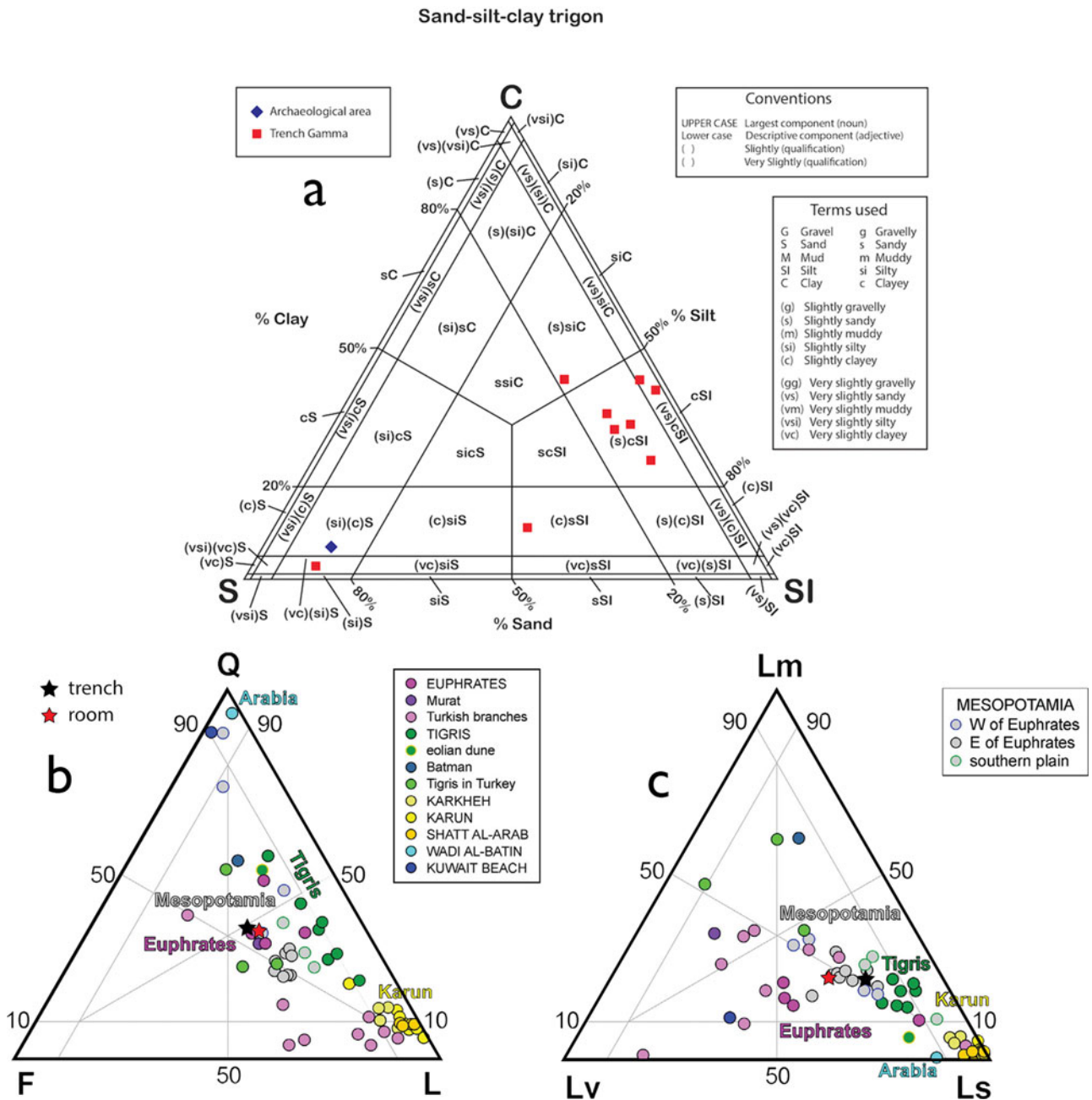
Samples from the trench Gamma and the archaeological site mainly consist of slightly clayey silt with a slight sandy component (Fig. 8a), having a feldspatho-quartzo-lithic sedimentary clastic signature (Fig. 8b, c). Monomineralic components of the sand-sized fraction include significant quartz and feldspar grains, with minor micas (biotite and muscovite) and heavy minerals (pyroxene, amphibole, epidote) (Fig. 9). Rock fragments are dominated by carbonate (micritic and sparitic) and siliciclastic (shale and chert) lithics, with common volcanic grains, having felsitic, lathwork to microlitic texture, and minor serpentinite and metamorphic lithic fragments.

Paleontological data

In the Abu Tbeirah samples, the ostracod assemblage is generally well preserved, with no evidence of dissolution and/or transport. This is confirmed by the occurrence of adult and juvenile separate valves and carapaces. The ostracods are represented by 12 different taxa, characteristic of freshwater to brackish waters (Fig. 10): *Cyprideis torosa*, *Ilyocypris bradyi*, *Ilyocypris monstifica*, *Stenocypris hislopi*, *Cypridopsis vidua*, *Vestalenula cylindrica*, *Darwinula stevensoni*, *Limnocythere inopinata*, *Candona neglecta*, *Pseudocandona* sp., *Heterocypris salina*, and *Potamocypris* sp.

The mollusks generally are poorly preserved and mostly represented by undeterminable fragments. They are represented by at least eight taxa: *Melanopsis (Melanopsis) praemorsum*, *Cerithidea (Cerithideopsilla) cingulata*, *Lymnaea (Radix) gr. auricularia*, *Bellamyia bengalensis*, *Gyraulus intermixtus*, *Lymnaea* spp., *Theodoxus* sp., and *Unio tigridis*. Bivalve fragments with characteristic striae on the shells are referable to *Corbicula fluminalis*.

The ostracod assemblages generally indicate a shallow-water environment with variable salinities. The assemblages from trenches Gamma and Delta point to a slow-flowing freshwater environment. The occurrence of the mollusk *Unio tigridis* confirms the slowly flowing freshwaters, typical of lakes and marsh channels, such as Typha marshes (Plaziat and Younis, 2005). The ostracod assemblage from the boreholes points to an oligohaline freshwater environment, rich in vegetation, with spring water input and episodes of increased salinities (>5‰), which, considering the general setting of the area (the internal sector of a delta plain), could be linked to a probable connection between the studied area and the sea through the intricate channels systems and/or enhanced aridity. This is confirmed by the dominance of smooth forms of *C. torosa* and the occurrence of *D. stevensoni*, a eurytopic cosmopolitan freshwater species that can tolerate high salinities and occasionally can be found at higher salinities (15‰, in Iran, Löffler, 1961), although commonly found in waters with salinities near 1‰. Scattered foraminifera (*Ammonia tepida*, *Haynesina germanica*), together with *Cerithidea (Cerithideopsilla) cingulata* and *Melanopsis (Melanopsis) praemorsum*, also occur in the sediment. The co-occurrence of *C. torosa* and *C. cingulata* indicates a connection with the sea and the tolerance to survive changing salinities, a trait typical of the two species. *Cerithidea cingulata* has been found previously in the vicinity of Ur (Soyer, 1961) and northwest of Nasiriyah (Annandale, 1918) during the Holocene, and was interpreted as an indicator of slightly saline lacustrine waters. It is considered an intertidal species, distributed around the Gulf (Iran and Arabian Peninsula).



Palaeobotanical data

The pollen study from Abu Tbeirah revealed that the majority of the samples were barren. A few pollen grains were found in bore-hole BHH (Area 5, southwestern sector) at 40 cm depth (Chenopodiaceae [chenopods] 4, Cyperaceae [sedges] 1 and *Myriophyllum spicatum* [spiked water-milfoil] 1), and at 550 cm (Chenopodiaceae [chenopods] 1, Typha [reeds] 4). In the investigated portion of the borehole BHA (near Area 2, northeastern sector), the following pollen types were found: *Pinus* (pine: 1) at 417 cm and 546 cm; cereal type and Poaceae (grasses) at 770 cm; Cyperaceae (sedges) and *Ephedra distachya* (jointfir)

type at 874 cm. Overall, the pollen indicators suggest a marshy environment.

A preliminary list of plant remains from the Abu Tbeirah dwelling contexts (Area 1 southeastern sector) includes interwoven fibers and mats, a palm stem, and some charred cereal grains (Fig. 11). Fragments of reed mats were retrieved from the floor of a building in connection with a hearth (D’Agostino et al., 2013; Celant and Magri, 2019). Intertwined reeds that also were found in domestic contexts and burials as baskets (Montorfani, 2019; Romano et al., 2021) were assigned to *Arundo donax* L., a common reed that is currently employed in southern Iraq as building

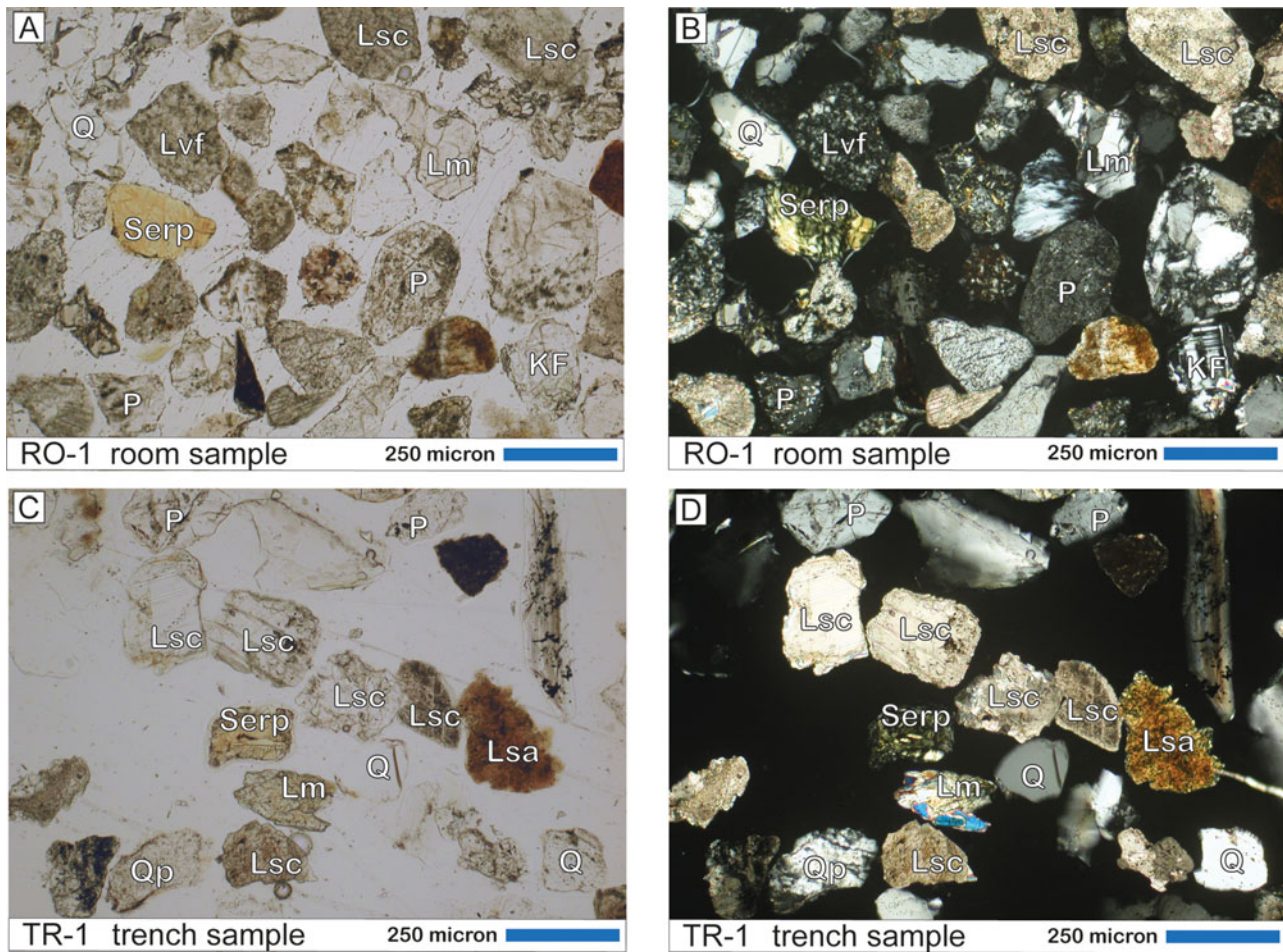


Figure 9. Thin sections showing photomicrographs of diagnostic grains in plain transmitted light (left) and crossed-polar (right) views of room sample RO-1 (A, B) and trench sample TR-1 (C, D). Q = monomineralic quartz; Qp = polyminalic quartz; KF = k feldspar; P = plagioclase; Serp = serpentinite grain; Lsc = carbonate lithic fragment; Lsa = argillite lithic fragments; Lm = metamorphic lithic fragment; Lvf = volcanic lithic fragment with felsitic texture.

and roofing material as well as a cover for floor surfaces. An unburned fragment of palm stem, ~15 cm long, was also identified as the date palm, *Phoenix dactylifera* L., and tentatively interpreted as the handle of a copper-alloy chisel found nearby (Area 1).

In the southeastern sector of the excavation (Area 1), evidence for agricultural activity of the Abu Tbeirah community is documented by a few charred cereal grains of barley (*Hordeum vulgare*) and einkorn wheat (*Triticum* cf. *T. monococcum*) that probably escaped from roasting processes (D'Agostino et al., 2015; Cereda and Romano, 2018; Celant and Magri, 2019).

Sedimentological data

The sedimentological description and the interpretation of the deposits took advantage of the remote sensing analysis of the area that enabled better definition of the depositional environments.

Trench Gamma description

Trench Gamma was excavated in 2018 in the northwestern sector of the site. It is NE-SW oriented, ~25 m long, and 1.2 m deep (Fig. 12a). With local textural change of the deposits in this trench, it is possible to recognize two main units separated by an erosional surface. The older unit (A) is constituted by olive

yellow very fine sand passing transitionally and laterally to brown clayey silt in which pieces of pottery and mollusk fragments are aligned, indicating transport by a unidirectional current. The younger unit (B) consists of a very dark gray, slightly sandy clayey silt (10–40 cm thick) passing downward and laterally to sandy clayey silt (~50 cm thick) with local occurrences of small lenses of yellow sands with evaporite minerals (essentially gypsum). Locally, gypcrete and calcrete, as well as root bioturbation of xerophyte plants and malacofauna constituted by terrestrial gastropods and fragments of bivalves, occur. In the central part of trench, this unit shows the presence of centimeter-scale alternation of grayish brown clayey silt and light yellowish sandy silt layers constituting the filling of a concave-up lenticular body 2 m wide and 35–40 cm thick. The top surface of this unit is the modern soil.

Trench Delta description

Trench Delta, which is 120 m southeast of trench Gamma, was excavated in 2018. It is NE-SW oriented, ~15 m long, and 1 m deep (Fig. 12b). This trench, as the previous one, can be subdivided into two main units separated by an erosional surface. The older unit (A) is constituted by light yellowish-brown sand showing a slightly inclined stratification dipping southwest. It is truncated by the erosional surface on which deposits of the

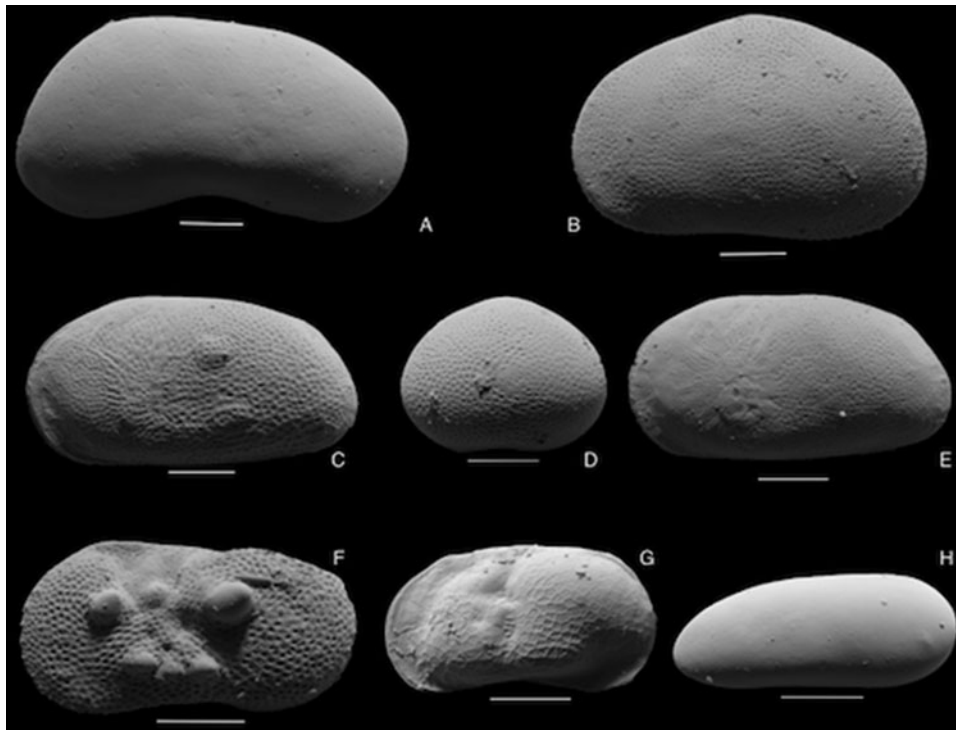


Figure 10. SEM photos of most abundant ostracod species. (A) *Candona neglecta*; (B) *Heterocypris salina*; (C) *Cyprideis torosa* (with nodes); (D) *Cypridopsis vidua*; (E) *Cyprideis torosa* (smooth form); (F) left valve of *Ilyocypris monstifrica*; (G) *Limnocythere inopinata*; (H) left valve of *Darwinula stevensoni*. Scale bars = 200 micron.

younger unit B are placed. Unit B is organized into three different subunits. From top to bottom, subunit B1 is the highest unit and is constituted by dark gray silty sand forming the present soil. Subunit B2 is constituted by light gray clayey silt in the upper part, while the lower part is a light reddish-brown clay with centimeter lenses of black organic matter (4572–4292 cal yr BP; Table 1). Along this passage, a layer of pottery fragments has been recognized. In B2, the presence of evaporite minerals forming a gypcrete some centimeters thick, and roots of xerophyte plants that produce pervasive bioturbation have been recognized locally. Pottery fragments, animal remains, and other artifacts are randomly distributed throughout B2, suggesting an influence of human activity during its deposition. Human activity is also recorded by a sharp V-shaped incision, ~50 cm deep, that cuts

subunit B2 at its right margin, which is filled by reddish to light gray clay with pottery fragments (subunit B3). The sharp V-shaped incision coincides with the erosional surface separating the Unit A from Unit B.

Trench Mal description

Trench Mal was excavated in 2019 in the southern sector outside the site, ~600 m from trenches Gamma and Delta. It is NW-SE oriented, 18 m long, and ~2 m deep (Fig. 12c). The trench is constituted by three units (from bottom to top): Unit C, ~50 cm thick, is constituted by clay with a pervasive presence of organic matter. The overlying unit B is separated from the underlying Unit C by an erosional surface, along which load structures and small muddy sandy clasts occur. Unit B is ~1 m thick, and shows a fining-upward trend characterized, from bottom to top, by a light gray fine sand that internally shows planar tabular cross-lamination (laminae apparently dip to SE) with rare centimeter mudstone clasts, passing upward to light red sandy silt with small-scale trough cross lamination, and farther upward to pedogenic light olive gray clay. Unit A is constituted by dark gray silty sand (Unit A) and is bounded below by an erosional surface. The top of Unit A is pedogenized and shows the presence of calcrete and gypcretes, as well as pervasive root bioturbation. Overall, this unit is <50 cm thick and shows small-scale channelized geometry having, in the more depressed sector, a lag constituted by shell fragments.

Borehole A description (BHA)

Borehole A was drilled in 2018 and is 18.8 m deep. The stratigraphy of this borehole can be subdivided into two portions. The upper portion, up to 9 m depth, is essentially constituted by mud with intercalations of thin sand beds, having an age

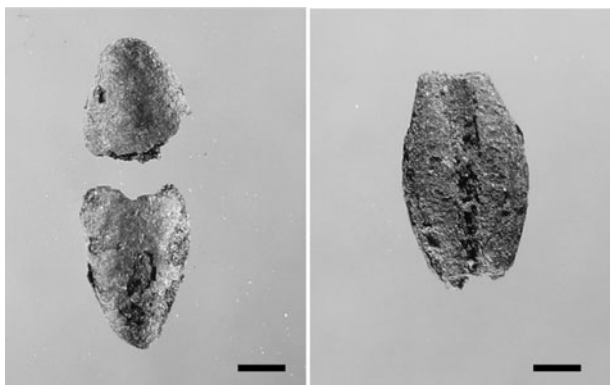


Figure 11. Caryopses of cereals from the pavement of Room 5, Building A—phase 2. Left: einkorn wheat (*Triticum* cf. *T. monococcum* L.); right: barley (*Hordeum vulgare* L.). Scale bar is 1 mm.



Figure 12. Orthophotos showing the trenches Gamma (a), Delta (b), and Mal (c) with their internal subdivision in units and subunits. The red and blue dots in trench Gamma indicate the positions of the samples utilized for compositional and paleontological analysis, respectively; the yellow dot in trench Delta indicates the position of the sample utilized for radiocarbon dating. Units A and B in both trenches Gamma and Delta are separated by the same discontinuity surface. The internal subdivisions of Trench Mal have no correspondence with those of Trench Gamma or Delta because they belong to a different environment and a different sedimentary body. The numbered squares and rectangles with different colors are control points for the photogrammetry software.

attributed to the Middle–Late Holocene, based on stratigraphic correlation with the radiocarbon dating samples of trench Delta (Table 1). Radiocarbon dates obtained from the sediments of BHA were rejected as contaminated by circulating carbon.

The lower portion, 9–18.8 m depth, is composed of thick sand beds and is attributed to the Late Pleistocene–Early Holocene. For our study, we utilized only the upper portion of the BHA, particularly the first 7 m (Fig. 13), for correlation with the other boreholes and trenches. This interval is comprised of dark yellowish-brown clay where centimeter-thick layers of organic matter and thin silty sand beds containing fragments of continental mollusks occur. Locally, thin and discontinuous calcrete and gyprocrete layers were recognized in the muddy deposits.

Borehole B description (BHB)

Borehole B was drilled in 2019 and is 5.20 m deep (Fig. 13). The deposits of this borehole consist of dark brown clay interbedded with thin olive gray silty sand beds, and medium light yellowish brown very fine sand beds. Thin layers of organic matter occur at depths between 1.5–2 m and between 4.5–5 m.

Borehole H description (BHH)

Borehole H was drilled in 2017 in the area where the archaeological excavation suggested the presence of a possible fluvial harbor (see following discussion) (Fig. 13). It is 6.35 m deep and was described in detail by Milli and Forti (2019). The deposits of this borehole are essentially composed of mud with alternating thin beds of silt and fine and very fine sand. Thin layers of organic matter occur at different levels within the deposits, while a thicker organic bed is present between 5–6 m depth. The radiocarbon date obtained from the sediments of BHH was rejected as contaminated by circulating carbon (Table 1).

DISCUSSION

The Late Holocene evolution of the lower Mesopotamian plain

Literature data and our investigations suggest that the Abu Tbeirah site developed during the most recent portion of the Holocene. At the beginning of this phase (ca. 6000 yr; Aqrawi, 2001; Pournelle, 2003; Kennet and Kennet, 2006; Milli and Forti, 2019), sea-level rise reached its maximum landward migration. Within the LMP, an estuarine shallow-marine/lagoon environment developed, stretched along the axis of the valley in the most depressed sector of the Mesopotamian plain. With the stabilization of sea level and the strongly reduced accommodation space, fluvial aggradation was at a minimum. The Tigris and Euphrates rivers moved towards the southeast, forming a shoreline along the alignment between the cities of Amarah and Nasiriyah (Aqrawi, 2001; Pournelle, 2003; Kennet and Kennet, 2006; Milli and Forti, 2019) with two well-developed deltas (Fig. 14). Remote sensing analysis of the investigated area indicates that these deltaic bodies had a lobate planform geometry with several distributary channels, at the end of which mouth bars formed, representing the loci of sand deposition (Coleman and Wright, 1975; Coleman and Prior, 1980; Galloway and Hobday, 1996, and references therein). Distributary channels were separated by interdistributary bays, where different environments, including marshes, swamps, floodplains, levees, and crevasse splays, occurred. All these features classify these deltas as tidal-influenced, river-dominated deltas.

Such delta geometry would have been favored by the morphology of the LMP at the end of the Holocene transgression: a large cul-de-sac open to the Persian Gulf where tides were probably amplified, allowing a strong interaction between fluvial and tidal processes (for more discussion on the delta

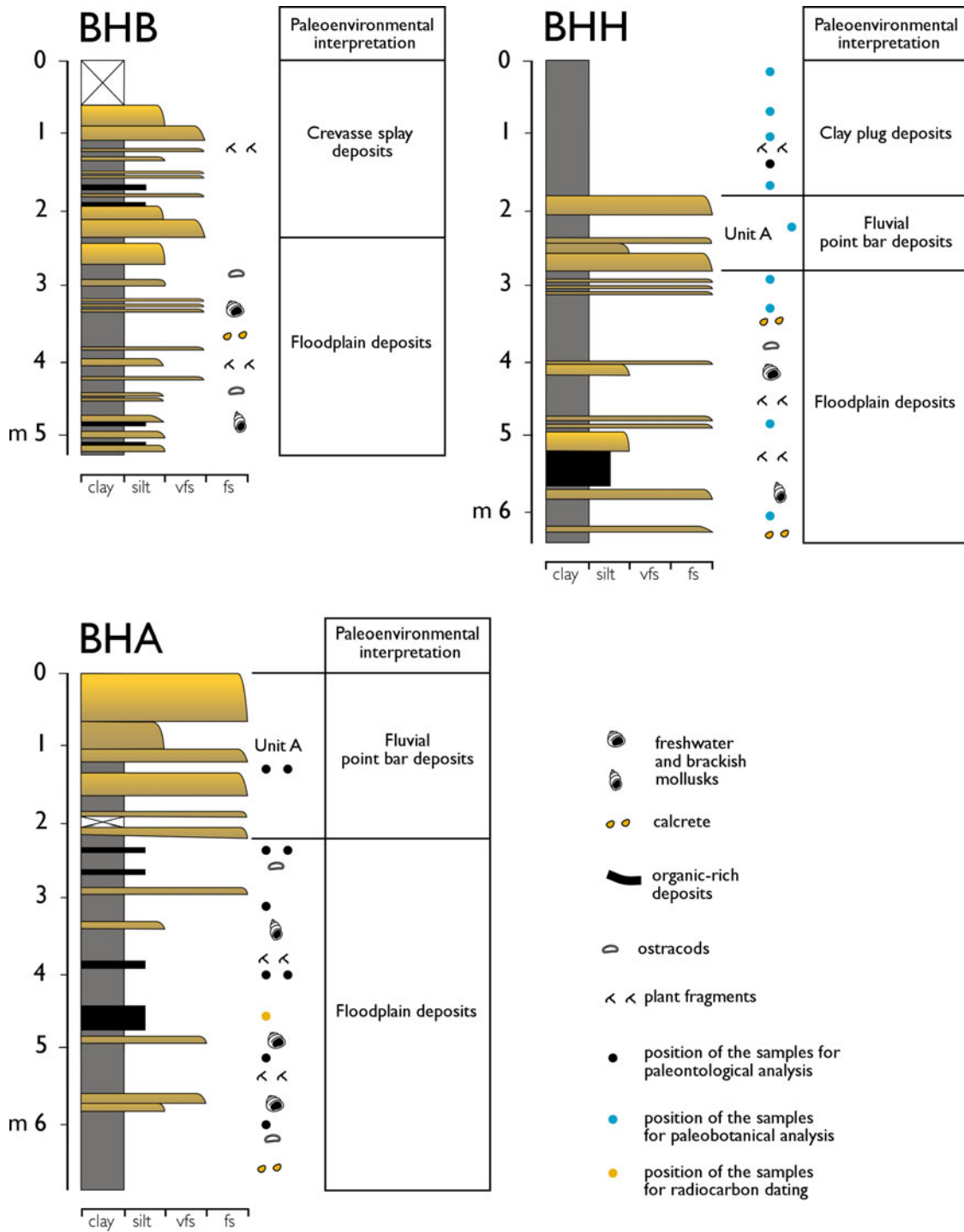


Figure 13. Stratigraphic columns of the BHA, BHB, and BHH cores showing the inferred depositional environments. The point-bar deposits of the BHA and BHH correspond to the deposits of Unit A in both of the Gamma and Delta trenches.

processes, see Giosan and Bhattacharya, 2005; Bhattacharya, 2006; Olariu and Bhattacharya, 2006; Ashworth et al., 2015; Hoitink et al., 2017).

From 6000 yr to ca. 5000 yr, the Tigris and Euphrates deltas prograded due to the development of a complex fluvial channel network under humid conditions (see Kay and Johnson, 1981; Bar-Matthews and Ayalon, 2011; Cheng et al., 2015; Sharifi et al., 2015; Nehme et al., 2018; Altaweel et al., 2019). This

probably favored avulsion processes, as well as the growth of human settlements through the increase of irrigated floodplain areas and agricultural productivity (Morozova, 2005; Kennet and Kennet, 2006; Engel and Brückner, 2021).

Starting from 5000 yr up to 4000 yr, a switch from humid to arid climatic conditions influenced the environments of LMP (Nehme et al., 2018; Engel and Brückner, 2021, and references therein). The progradation of the Tigris and Euphrates deltas

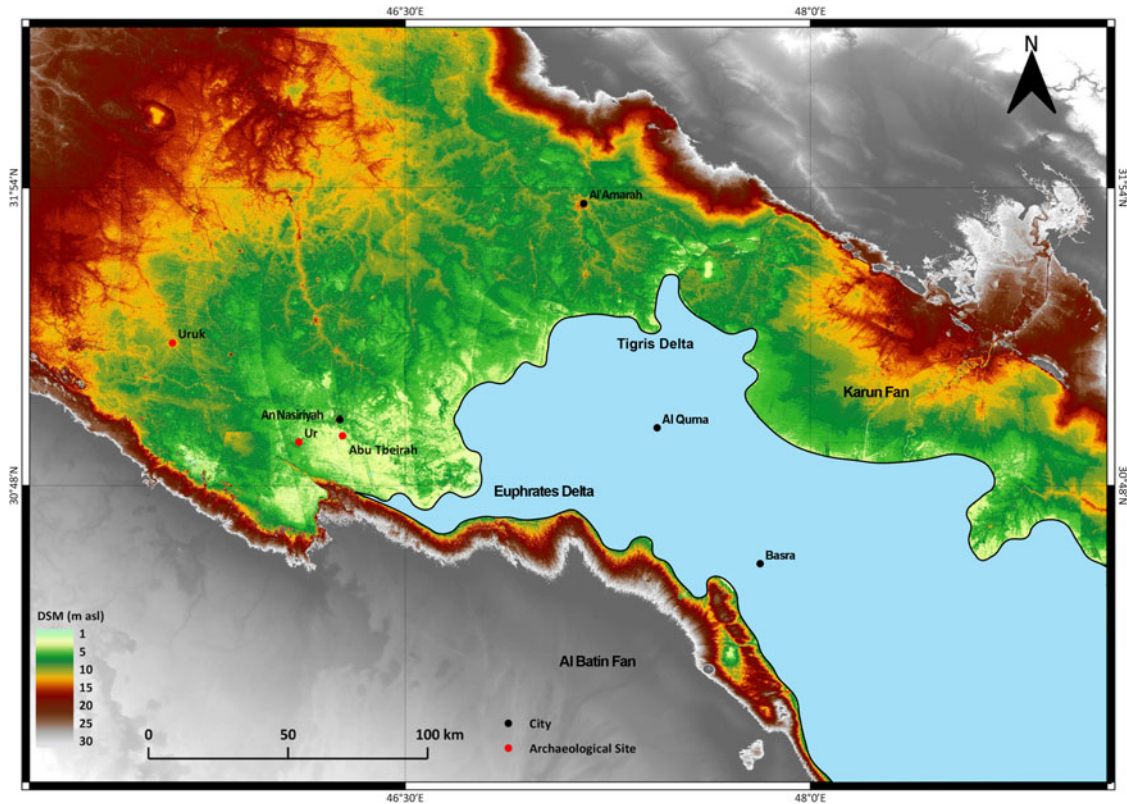


Figure 14. Suggested position of the Persian Gulf coastline between 5000–4000 years ago. Note the location of the Abu Tbeirah site in the upper delta plain of the Euphrates River. Map modified from AW3D30 Digital Surface Model (DSM), available on the Japan Aerospace Exploration Agency (JAXA, 2020).

slowed significantly and then ceased, the complex of multiple fluvial channels was gradually abandoned, and the present fluvial pattern with the periodic shifting of the river courses, floodplain aggradation, and enhanced soil-formation started to develop (see also Sanlaville, 1989, 2003; Aqrawi, 1995a, 2001; Morozova, 2005; Jerolmack and Mohrig, 2007; Jerolmack, 2009; Pennington et al., 2016). These changes were the result of: (1) neotectonic movement (essentially the growth of subsurface faults and anticlines, as well as salt-diapiric structures; Baltzer and Purser, 1990; Al-Sakini, 1993; Fouad and Sissakian, 2011; Sissakian et al., 2018, 2020); (2) development of the alluvial fans occurring along the margins of the LMP (see for example Baltzer and Purser, 1990; Sissakian et al., 2014); (3) climatic changes that produced the hydrological variability of the Tigris and Euphrates rivers; and (4) human activities that exploited the natural waterways for agricultural irrigation and fishing, especially in areas where crevasse splays commonly developed (Pournelle, 2003; Morozova, 2005; Kennett and Kennett, 2006; Jotheri et al., 2016, 2018; Jotheri and Allen, 2020).

In the Ahwar area, freshwater conditions have persisted since ca. 3000 yr (see Aqrawi and Evans, 1994; Altweel et al., 2019). The Gulf probably attained its present configuration ca. AD 1000 as a result of the progradation, south of Basrah, of the Shatt Al-Arab delta (Aqrawi, 2001; Al-Hamad et al., 2017; Bogemans et al., 2017). At present, the tidal-influenced Shatt-al-Arab delta is mainly supplied by the Karun River, whose sediments are mainly derived from the eastern Zagros Mountains and from small rivers draining the Arabian Platform (see Baltzer and Purser, 1990; Garzanti et al., 2016, for a more detailed study about the sediment provenance of the

Mesopotamian foreland basin). During this last period, continental deposition developed, being characterized by extensive floodplain environments with large marshland areas where intertwined sinuous channels, levees, crevasse splays, and flood basins occurred and where the rivers deposited most of their load. These characters reflect the important climate changes that occurred in the LMP at the transition between the Middle and Late Holocene and during the Late Holocene, which conditioned human activities and development of the many archaeological sites of this area (Weiss et al., 1993; Pournelle, 2003; Morozova, 2005; Kennett and Kennett, 2006; Wilkinson et al., 2015; Engel and Brückner, 2021).

Paleoenvironment of the area surrounding Abu Tbeirah

Our results derived from compositional, paleontological, paleobotanical and sedimentological data are consistent with the published data on the environmental and depositional settings of the LMP indicating for the Abu Tbeirah a flooded marshland environment with fluvial channels and with the presence of well-developed crevasse splays, the existence of which is a good indicator of seasonal flooding and avulsion processes (Bristow et al., 1999; Iacobucci et al., 2020, with references therein). Several studies also have pointed out that these features characterize the best and most suitable riverine environment for living and for the formation of systematically irrigated farms (Wilkinson et al., 2015).

The compositional characters of our samples and their comparison with detrital modes from the modern Euphrates, Tigris,

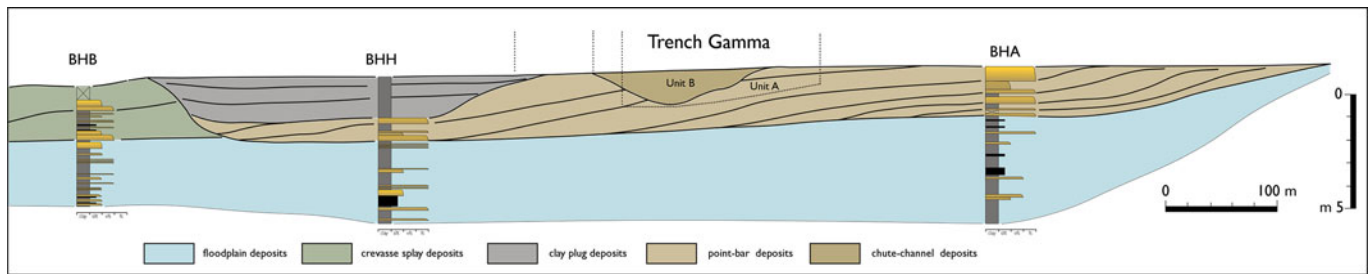


Figure 15. Detailed correlation panel showing the reconstructed geometry and the stratigraphic relationships of the point bar and chute channel developed in the Abu Tbeirah archaeological site. See Figure 7 for location of cross section.

and Karun fluvial sands (see Garzanti et al., 2016) suggest an intermediate composition between the Euphrates and Tigris samples, and within the range of Mesopotamian floodplain sand composition (see Fig. 8b, c). In particular, the provenance of the studied samples reflects reworking of sedimentary, volcanoclastic, and metamorphic basement source rocks from the Anatolia-Zagros orogen and suggests extensive mixing and homogenization of floodplain sediments as a result of fluvial dynamics (e.g., avulsion episodes, lateral migration and repeated bifurcation of trunk-river channels). The micropaleontology results indicate an influence of slightly saline water in the paleoenvironmental reconstruction. The ostracod and mollusk assemblages indicate a shallow-water environment, rich in vegetation, with spring water input and some episodes of increased salinity (>5‰) (see also Al-Sheikly et al., 2017; Hassan, 2018), which, considering the general setting of the area (the internal sector of a delta plain), could be linked to a probable connection between the studied area and the sea through the intricate channel system.

It is here suggested that, considering the distance of the site from the coastline, the morphological confinement of the Gulf basin, and the faunal assemblage, tides also influenced sedimentation in the study area. Tidal effects are generally evinced in the characters of beds forming the filling of the fluvial channels that probably record neap-spring cyclicity and changes of river discharge (see also Dalrymple et al., 2015; Keevil et al., 2015).

This depositional environment is also confirmed by the pollen analysis of the sectors surrounding the Abu Tbeirah site (see Al-Ameri et al., 2005, 2011; Al-Ameri and Jassim, 2011; Al-Ameri and Al-Dolaymi, 2013; Kumar, 2015), characterized by the presence of Poaceae and Palmae, and by two distinct environments: a permanently flooded marshland with abundant *Typha* and other marshy plants, associated with deposition of peat and/or organic clay; and a partially dry marshland where *Typha* is missing, but abundant chenopods are found, indicating a salt-rich substratum.

The results of sedimentological analysis, together with the remote sensing, compositional, paleontological, and paleobotanical analyses have allowed better interpretation of the deposits from the trench and boreholes near the Abu Tbeirah site. In particular, we produced a detailed correlation panel utilizing the stratigraphy of the upper portion of borehole A, trench Gamma, and boreholes H and B (Fig. 15). Such correlation allowed us to identify several types of deposits whose sedimentological characters indicate a floodplain with marsh environment, where a sinuous channel with associated crevasse splay bodies occurred.

The geometry and type of stratification recognized in the Gamma and Delta trenches allowed us to correlate their deposits, because of the correspondence between units A and B of both trenches. These units are also separated by the same discontinuity surface. Correlation with the boreholes allowed us to reconstruct the accretionary units of a point bar (deposits of the point bar coincide with unit A of the Gamma and Delta trenches), with bank erosion located on the right side of the correlation panel (see Fig. 15). Currently, this sector shows a well-developed clay plug (upper portion of the BHH) that constitutes filling of the main sinuous channel after its abandonment, following a chute cut-off (Figs. 7, 15). The abandoned channel became a shallow water pond (ox-bow lake), ~1 km long and 80 m wide, that was at least partially utilized by people as a protected fluvial harbor, as revealed by the archaeological excavation.

In our opinion, the chute channel (sector of trench Gamma) was present when the initial sinuous Abu Tbeirah channel was active, but it was probably dry for most of the time and became active only during flood events and in other high-water stage conditions. The chute cut-off probably occurred during a strong flood event and after a progressive abandonment of the main channel, a process that would result in a reduction of crevasse splay area associated with the initial sinuous Abu Tbeirah channel (Fig. 7A). This process in turn was probably related to a reduction of the sediment supply due to climate change, although human intervention cannot be ruled out (e.g., Tamburrino, 2010). The chute channel was probably not very wide immediately after the cut-off, but it might have been enlarged successively at the expense of the original channel.

The stratigraphy and the sedimentological characteristics of deposits, together with field observations, indicate that borehole BHB occupies the proximal sector of a crevasse splay and trench Mal its middle sector (Fig. 7). These crevasse splays form lobate bodies (fan shaped in plan with an upward convexity) with a distributive multi-channel system (e.g., Bridge, 2004; Marriott, 2004). As previously described, remote sensing analysis allowed us to identify at least eight crevasse splays connected to the fluvial dynamics of the initial sinuous Abu Tbeirah channel, whose dimensions decrease, moving from NW to SE. Most of these bodies form a hierarchy of composite bodies that are stacked in a compensational manner (see also Iacobucci et al., 2020). Our observations suggest that proximal feeder-channels controlled the evolution of the lobe and the vertical arrangement of the crevasse splays.

The previous considerations, as well as the pottery collected within the Abu Tbeirah fluvial channels and the radiocarbon dating (4572–4292 cal yr BP, Unit B, trench Delta), seem to confirm

that the crevasse splays formed before the chute cut-off (i.e., before of 4400 yr) and that the watercourses were used at least since the beginning of the second half of the third millennium BC and for a period of time of ca. 200–400 years, before the climate change occurring at the transition from Middle (Northgrippian) to Late Holocene (Meghalayan). Ethnographic comparison with the Ma'dain of the Iraqi Marshes suggests that this newly formed shallow-water basin (ox-bow lake) was used not only as a fluvial harbor, but also for all the city activities connected to water (see also Rost et al., 2011).

CONCLUSIONS

Based on our data, our main conclusions are summarized below.

About 5000 years ago, the Persian Gulf coastline was characterized by the presence of Euphrates and Tigris tidal-influenced, river-dominated deltas that prograded seaward from the end of the post-glacial sea-level rise (ca. 6000 yr) up to ca. 5000 yr, with conditions of stillstand or slight sea-level rise during wet conditions. Starting from 5000 yr up to 4000 yr, a switch from humid to arid climatic conditions with a progressive increase in temperature and annual evaporation rates influenced the environments of LMP. Due to the decrease of water and sediment supply, progradation of the Euphrates and Tigris deltas slowed significantly, and between 4000–3000 yr, they prograded slowly only as swampy inland deltas before being covered by the most recent Holocene alluvial deposits. The marine Euphrates delta, with its well-developed upper delta plain characterized by distributary channels with low and immature levees, provided the environments where the settlement of Abu Tbeirah developed, located ~30 km inland from the Gulf coastline.

The Abu Tbeirah site developed along an originally sinuous distributary channel flowing in a wetland floodplain environment with marshes and crevasse splays. This channel, which was abandoned following a chute cut-off, formed an isolated shallow-water basin utilized by the inhabitants of Abu Tbeirah as a protected fluvial harbor and for other human activities, including as a water reservoir during arid periods or as a “compensation basin” during floods.

Our multidisciplinary research approach shows how the Sumerians managed this peculiar environment and exploited the water resources as an important subsistence strategy. This suggests that during the Sumerian period, and probably during the previous Ubaid and Uruk periods, the human communities experimented with aquatic activities, which helped to mobilize food surplus between settlements. Such consideration highlights that during the Middle and Late Holocene, human cultural evolution in southern Mesopotamia was strongly influenced by important environmental changes, induced by global eustatic sea-level rise and climate change (from humid to arid conditions). This changed aquatic resources (fish in particular), but more importantly induced an increase of agriculture, revealed by construction of several canals and irrigation systems. Human activities modified the landscape and the environment, but most of all these environmental changes modified the lifestyle of the communities in ways that ultimately favored the emergence of highly centralized, urban-based states.

Acknowledgments. The authors thank the senior editor Derek Booth and the associate editor John Dodson as well as the three anonymous reviewers for their discussion, suggestions, and constructive revisions that led to improvements of the manuscript. We thank the colleagues of the Iraqi State

Board for Antiquities and Heritage for all the assistance and fundamental support to our common work at Abu Tbeirah. Abu Tbeirah's research is funded by SAPIENZA Università di Roma and by the Italian Ministry of Foreign Affairs. The geoarchaeological work, in particular the research on the Harbor, is supported by the Franco Bardelli Foundation.

REFERENCES

- Adams R.M. 1965. *Land Behind Baghdad: A History of Settlement on the Diyala Plains*. Chicago, University of Chicago Press.
- Adams R.M. 1981. *Heartland of Cities: Surveys of Ancient Settlement and Land Use on the Central Floodplain of the Euphrates*. Chicago, University of Chicago Press.
- Agard, P., Omrani, J., Jolivet, L., Mouthereau, F., 2005. Convergence history across Zagros (Iran): constraints from collisional and earlier deformation. *International Journal of Earth Sciences* **94**, 401–419.
- Alavi, M., 2004. Regional stratigraphy of the Zagros fold-thrust belt of Iran and its foreland evolution. *American Journal of Science* **304**, 1–20.
- Alavi, M., 2007. Structures of the Zagros fold-thrust belt in Iran. *American Journal of Science* **307**, 1064–1095.
- Al-Ameri, T.K., Al-Dolaymi, A.S.F., 2013. Human settlements adapted to environmental changes through the Paleolithic and Neolithic times in West Iraq. *Arabian Journal of Geosciences* **6**, 2951–2960.
- Al-Ameri, T.K., Jassim, S.Y., 2011. Environmental changes in the wetlands of southern Iraq based on palynological studies. *Arabian Journal of Geosciences* **4**, 443–461.
- Al-Ameri, T.K., Al-Tawash, B.S., Al-Rawi, Y.T., 2005. Pollen evidence of late Quaternary vegetation and inferred climatic changes of Lake Razzaza, Western Iraqi Desert. *Iraqi Bulletin of Geology and Mining* **1**, 1–13.
- Al-Ameri, T.K., Jasim, S.Y., Al-Khafaji, A.J.S., 2011. Middle Paleolithic to Neolithic cultural history of North Iraq. *Arabian Journal of Geosciences* **4**, 945–972.
- Algaze G. 2008. *Ancient Mesopotamia at the Dawn of Civilization: the Evolution of an Urban Landscape*. Chicago, University of Chicago Press.
- Al-Hamad S., Albadran B., Pournelle J. 2017. Geological history of Shatt Al-Arab River, south of Iraq. *International Journal of Science and Research* **6**, 2029–2039.
- Al-Kadhimi, J.M.A., Sissakian, V.K., Fattah, A.S., Deikran, D.B., 1996. *Tectonic Map of Iraq, scale 1:1,000,000, 2nd ed.* Iraq Geological Survey Publication, Baghdad, Iraq.
- Al-Sakini, J.A., 1993. *New Look on the History of Old Tigris and Euphrates Rivers, in the Light of Geological Evidences. Recent Archaeological Discoveries and Historical Sources*. Oil Exploration Co., Baghdad, Iraq, 93 pp. [in Arabic]
- Al-Sheikly, S.S., Al-Jumaily, W.A., Al-Ka'abi, F.S., Al-Shehmany, Z.K., Owen, M.A., 2017. Late Pleistocene–Holocene paleoecology of southern Mesopotamia, Iraq. *Journal of Science* **58**, 1856–1873.
- Altaweel, M., Marsh, A., Jotheri, J., Hritz, C., Fleitmann, D., Rost, S., Lintner, S.F., et al., 2019. New Insights on the role of environmental dynamics shaping southern Mesopotamia: from the pre-Ubaid to the early Islamic period. *Iraq* **81**, 23–46.
- Annandale, T.N., 1918. Freshwater shells from Mesopotamia. *Records of the Indian Museum, Calcutta* **15**, 159–170.
- Aqrabi, A.A.M., 1995a. Correction sedimentation rates for mechanical compaction: the Tigris and Euphrates Delta, lower Mesopotamia. *Marine and Petroleum Geology* **12**, 409–416.
- Aqrabi, A.A.M., 1995b. Brackish-water and evaporitic Ca-Mg carbonates in the Holocene lacustrine/deltaic deposits of southern Mesopotamia. *Journal of the Geological Society* **152**, 259–268.
- Aqrabi, A.A.M., 2001. Stratigraphic signatures of climatic change during the Holocene evolution of the Tigris-Euphrates Delta, lower Mesopotamia. *Global and Planetary Change* **28**, 267–283.
- Aqrabi, A.A.M., Evans, G., 1994. Sedimentation in the lakes and marshes (Awhar) of the Tigris-Euphrates Delta, southern Mesopotamia. *Sedimentology* **41**, 755–776.
- Ashworth, P.J., Best, J.L., Parsons, D.R. (Eds.), 2015. *Fluvial-Tidal Sedimentology*. Developments in Sedimentology **68**, 634 pp.

- Baltzer, F., Purser, B.H.**, 1990. Modern alluvial fan and deltaic sedimentation in a foreland tectonic setting: the Lower Mesopotamian Plain and the Arabian Gulf. *Sedimentary Geology* **67**, 175–197.
- Bar-Matthews, M., Ayalon, A.**, 2011. Mid-Holocene climate variations revealed by high-resolution speleothem records from Soreq Cave, Israel and their correlation with cultural changes. *The Holocene* **2**, 163–171.
- Bhattacharya, J.P.**, 2006. Deltas. In: Posamentier, H.W., Walker R.G. (Eds.), *Facies Models Revisited*. SEPM (Society for Sedimentary Geology), Special Publication 84, pp. 237–292.
- Blott, S.J., Pye, K.**, 2012. Particle size scales and classification of sediment types based on particle size distributions: review and recommended procedures. *Sedimentology* **59**, 2071–2096.
- Bogemans, F., Boudin, M., Janssens, R., Baeteman, C.**, 2017. New data on the sedimentary processes and timing of the initial inundation of Lower Khuzestan (SW Iran) by the Persian Gulf. *The Holocene* **27**, 613–620.
- Bridge, J.S.**, 2004. Alluvium. In: Goudie, A.S. (Ed.), *Encyclopedia of Geomorphology, 1st ed.* Routledge, London, pp. 19–21.
- Bridge, J., Demicco, R.**, 2008. *Earth Surface Processes, Landforms, and Sediment Deposits*. Cambridge University Press, New York, USA.
- Bristow, C.S., Skelly R.L., Ethridge F.G.**, 1999. Crevasse splays from the rapidly aggrading, sand-bed, braided Niobrara River, Nebraska: effect of base level rise. *Sedimentology* **46**, 1029–1048.
- Burns, C., Mountney, N.P., Hodgson, D.M., Colomera, L.**, 2017. Anatomy and dimensions of fluvial crevasse-splay deposits: examples from the Cretaceous Castlegate Sandstone and Neslen Formation, Utah, USA. *Sedimentary Geology* **351**, 21–35.
- Celant, A., Magri, D.**, 2019. Palaeoenvironment, climate and land use in southern Mesopotamia/Nasiriyah area. In: Romano L, D'Agostino F. (Eds.), *Abu Tbeirah Excavations I. Area 1: Last Phase and Building A—Phase 1*. Sapienza Università Editrice, Roma, pp. 39–47.
- Cereda, S., Romano, L.**, 2018. Peering into the dusty corners: micro-debris analysis and use of space at the site of Abu Tbeirah (Nasiriyah, Iraq). *Iraq* **80**, 79–111.
- Cheng, H., Sinha, A., Verheyden, S., Nader, F.H., Li, X.L., Zhang, P.Z., Yin, L., et al.**, 2015. The climate variability in northern Levant over the past 20,000 years. *Geophysical Research Letters* **42**, 8641–8650.
- Cole, S.**, 1994. Marsh formation in the Borsippa region and the course of the lower Euphrates. *Journal of Near Eastern Studies* **53**, 81–109.
- Cole, S., Gasche, H.**, 1998. Second- and first-millennium BC rivers in northern Babylonia. In: Gasche, H., Tanret, M. (Eds.), *Mesopotamian History and Environment, Memoirs V—Changing Watercourses in Babylonia. Towards a Reconstruction of the Ancient Environment in Lower Mesopotamia*. Memoirs V, 1–64. Ghent, Belgium and Chicago, University of Ghent and Oriental Institute of the University of Chicago.
- Coleman, J.M., Prior, D.B.**, 1980. *Deltaic Sand Bodies*. American Association of Petroleum Geologists. Continuing Education Course Note, Series 15.
- Coleman, J.M., Wright, L.D.**, 1975. Modern river deltas: variability processes and sand bodies. In: Broussard, M.L. (Ed.), *Deltas*. Houston Geological Society, Houston, Texas, pp. 99–150.
- D'Agostino, F., Romano, L.**, 2020a. Seven excavation campaigns at Abu Tbeirah. In: Otto, A., Herles, M., Kaniuth, K., Korn, L., Heidenreich, A. (Eds.), *Proceedings of the 11th International Congress on the Archaeology of the Ancient Near East: vol. 2: Field Reports, Islamic Archaeology*. Harrassowitz Verlag, Wiesbaden, Germany, pp. 69–80.
- D'Agostino, F., Romano, L.**, 2020b. Two new inscribed bricks from Abu Tbeirah (southern Iraq). In: Arkhipov, I., Kogan, L., Koslova, N. (Eds.), *The Third Millennium. Studies in Early Mesopotamia and Syria in Honor of Walter Sommerfeld and Manfred Krebernik*. Series: Cuneiform Monographs, vol. 50. Brill, Leiden, Boston, pp. 259–269.
- D'Agostino, F., Romano, L., Ghanim, K. A., Tafuri, M.A.**, 2013. Abu Tbeirah. Preliminary report of the second campaign (October–December 2012). *Rivista degli Studi Orientali* **86**, 69–92.
- D'Agostino, F., Romano, L., Ghanim, K. A.**, 2015. Abu Tbeirah, Nasiriyah (southern Iraq). Preliminary report on the 2013 excavation campaign. In: Biga, M.G., Cordoba, J.M., del Cerro, C., Torres, E. (Eds.), *Homenaje a Mario Liverani, Fundador de Una Ciencia Nueva (II)*. ISIMU 13, Madrid, pp. 209–221.
- Dalrymple, R.W., Kurcinka, C.E., Jablonski, B.V.J., Ichaso, A.A., Mackay, D.A.**, 2015. Deciphering the relative importance of fluvial and tidal processes in the fluvial-marine transition. In: Ashworth, P.J., Best, J.L., Parsons, D.R. (Eds.), *Fluvial-Tidal Sedimentology*. Developments in Sedimentology **68**, pp. 3–45.
- Dercourt, J., Zonenshain, L.P., Ricou, L.-E., Kazmin, V.G., Le Pichon, X., Knipper, A.L., Grandjacquet, et al.**, 1986. Geological evolution of the Tethys belt from the Atlantic to the Pamirs since the Lias. *Tectonophysics* **123**, 241–315.
- Di Giacomo, G., Scardozzi, G.**, 2012. Multitemporal high-resolution satellite images for the study and monitoring of an ancient Mesopotamian city and its surrounding landscape: the case of Ur. *International Journal of Geophysics* 2012, ID 716296. <https://doi.org/10.1155/2012/716296>.
- Engel, M., Brückner, H.**, 2021. Holocene climate variability of Mesopotamia and its impact on the history of civilisation. In: Ehlers, E., Amirpur K. (Eds.), *Middle East and North Africa*. Series: Climate and Culture, vol. 6. Brill, pp. 77–113.
- Fouad, S.F.A.**, 2012. *Tectonic Map of Iraq, scale 1:1,000,000, 3rd edition*. Iraq Geological Survey Publications, Baghdad, Iraq.
- Fouad, S.F.A., Sissakian, V.K.**, 2011. Tectonic and structural evolution of the Mesopotamia Plain. *Iraqi Bulletin of Geology and Mining, Special Issue 4*, 33–46.
- Galloway, W.E., Hobday, D.K.**, 1996. *Terrigenous Clastic Depositional Systems. Applications to Petroleum, Coal, and Uranium Exploration*. Springer-Verlag, New York.
- Garzanti, E.**, 2019. Petrographic classification of sand and sandstone. *Earth-Science Reviews* **192**, 545–563.
- Garzanti, E., Vezzoli, G.**, 2003. A classification of metamorphic grains in sands based on their composition and grade. *Journal of Sedimentary Research* **73**, 830–837.
- Garzanti, E., Al-Juboury, A.I., Zoleikhaei, Y., Vermeesch, P., Jotheri, J., Akkoca, D.B., Obaid, A.K., et al.**, 2016. The Euphrates-Tigris-Karun river system: provenance, recycling and dispersal of quartz-poor foreland-basin sediments in arid climate. *Earth-Science Reviews* **162**, 107–128.
- Giosan, L., Bhattacharya, J.P.**, (Eds.), 2005. *River Deltas—Concepts, Models, and Examples*. SEPM (Society for Sedimentary Geology), Special Publication 83.
- Gulliford, A.R., Flint, S.S., Hodgson, D.M.**, 2017. Crevasse splay processes and deposits in an ancient distributive fluvial system: the lower Beaufort Group, South Africa. *Sedimentary Geology* **358**, 1–18.
- Hammer, E.**, 2019. The city and landscape of Ur: an aerial, satellite, and ground reassessment. *Iraq* **81**, 173–206.
- Hassan, M.**, 2018. Habitat requirements of Ostracoda from water bodies in middle of Iraq. *Biochemical and Cellular Archives* **18**, 2197–2202.
- Heyvaert, V., Baeteman, C.**, 2008. A Middle to Late Holocene avulsion history of the Euphrates River: a case study from Tell Ed-Der, Iraq, lower Mesopotamia. *Quaternary Science Reviews* **2**, 2401–2410.
- Heyvaert, V.M.A., Walstra, J., Verkinderen, P., Weerts, H., Ooghe, B.**, 2012. The role of human interference on the channel shifting of the Karkheh River in the Lower Khuzestan plain (Mesopotamia, SW Iran). *Quaternary International* **251**, 52–63.
- Hoitink, A.J.F., Wang, Z.B., Vermeulen, B., Huismans, Y., Kästner, K.**, 2017. Tidal controls on river delta morphology. *Nature Geoscience* **10**, 637–645.
- Hritz, C., Pournelle, J.**, 2016. Deltaic resilience, inherited practice, and millennial-scale sustainability in an urbanized landscape. In: Foster, H.T., II, Paciulli, L.M., Goldstein, D.J. (Eds.), *Viewing the Future in the Past*. The University of South Carolina Press, Columbia, South Carolina, pp. 59–85.
- Hritz, C., Wilkinson, T.J.**, 2006. Using shuttle radar topography to map ancient water channels in Mesopotamia. *Antiquity* **80**, 415–424.
- Iacobucci, G., Troiani, F., Milli, S., Mazzanti, P., Piacentini, D., Zocchi, M., Nadali, D.**, 2020. Combining satellite multispectral imagery and topographic data for the detection and mapping of fluvial avulsion processes in lowland areas. *Remote Sensing* **12**, 2243. <https://doi.org/10.3390/rs12142243>.
- Ingersoll, R.V., Bullard, T.F., Ford, R.L., Grimm, J.P., Pickle, J.D., Sares, S.W.**, 1984. The effect of grain size on detrital modes: a test of the

- Gazzi-Dickinson point-counting method. *Journal of Sedimentary Petrology* **54**, 103–116.
- Jassim, S.Z., Goff, J.C., 2006. *Geology of Iraq*. Dolin, Prague and Moravian Museum, Brno, Czech Republic.
- Jerolmack, D.J., 2009. Conceptual framework for assessing the response of delta channel networks to Holocene sea level rise. *Quaternary Science Review* **2**, 1786–1800.
- Jerolmack, D.J., Mohrig, D., 2007. Conditions for branching in depositional rivers. *Geology* **35**, 463–466.
- Jotheri, J., 2018. Recognition criteria for canals and rivers in the Mesopotamian floodplain. In: Zhuang Y., Altaweel M. (Eds.), *Water Societies and Technologies from the Past and Present*. UCL Press, London, pp. 111–126.
- Jotheri, J., 2019. The environment and landscape archaeology of the Abu Tbeirah region. In: Romano L., D'Agostino, F. (Eds.), *Abu Tbeirah Excavations I. Area 1 Last Phase and Building A—Phase 1*. Sapienza Università Editrice, Roma, pp. 49–58.
- Jotheri, J., Allen, M.B., 2020. Recognition of ancient channels and archaeological sites in the Mesopotamian floodplain using satellite imagery and digital topography. In: Lawrence, D., Altaweel, M., Philip, G. (Eds.), *New Agendas in Remote Sensing and Landscape Archaeology in the Near East. Studies in Honour of Tony J. Wilkinson*. Archaeopress Publishing Ltd, Oxford, UK, pp. 283–305.
- Jotheri, J., Allen, M.B., Wilkinson, T.J., 2016. Holocene avulsions of the Euphrates River in the Najaf area of western Mesopotamia: impacts on human settlement patterns. *Geoarchaeology* **31**, 175–193.
- Jotheri, J., Altaweel, M., Tuji, A., Anma, R., Pennington, B., Rost, S., Watanabe, C., 2018. Holocene fluvial and anthropogenic processes in the region of Uruk in southern Mesopotamia. *Quaternary International* **483**, 57–69.
- Karanovic, I., 2012. *Recent Freshwater Ostracods of the World: Crustacea, Ostracoda, Podocopida*. Springer, Heidelberg, 610 pp.
- Kay, P.A., Johnson D.L., 1981. Estimation of Tigris-Euphrates streamflow from regional paleoenvironmental proxy data. *Climatic Change* **3**, 251–263.
- Keevil, C.E., Parsons, D.R., Keevil, G.M., Ainsley, M., 2015. Three-dimensional meander bend flow within the tidally influenced fluvial zone. In: Ashworth, P.J., Best, J.L., Parsons, D.R. (Eds.), *Fluvial-Tidal Sedimentology*. Developments in Sedimentology **68**, pp. 127–148.
- Kennett, D.J., Kennett, J.P., 2006. Early state formation in southern Mesopotamia: sea levels, shorelines, and climate change. *Journal of Island & Coastal Archaeology* **1**, 67–99.
- Kumar, A., 2015. Environmental changes in the wetlands of southern Iraq based on palynological studies: Comments. *Arabian Journal of Geosciences* **8**, 4287–4289.
- Löffler, H., 1961. Beiträge zur Kenntnis der iranischen Binnengewässer II. Regional-limnologische Studie mit besonderer Berücksichtigung der Crustaceenfauna. *Internationale Revue der Gesamten Hydrobiologie* **46**, 309–406.
- Magri, D., Di Rita, F., 2015. Archaeopalynological preparation techniques. In: Yeung, E.C.T., Stasolla, C., Sumner, M.J., Huang, B.Q. (Eds.), *Plant Microtechniques and Protocols*. Springer International Publishing, Cham, Switzerland, pp. 495–506.
- Marriott, S.B., 2004. Floodplain. In: Goudie, A.S. (Ed.), *Encyclopedia of Geomorphology, 1st ed.* Routledge, London, pp. 381–384.
- Meisch, C., 2000. Freshwater Ostracoda of western and central Europe. In: Schwoerbel, J., Zwick, P. (Eds.), *Süßwasserfauna von Mitteleuropa 8/3*. Spektrum Akademischer Verlag, Heidelberg, Berlin.
- Milli, S., Forti, L., 2019. Geology and palaeoenvironment of Nasiriyah area/southern Mesopotamia. In: Romano L., D'Agostino F. (Eds.), *Abu Tbeirah Excavations I. Area 1 Last Phase and Building A—Phase 1*. Sapienza Università Editrice, Roma, pp. 19–33.
- Montorfani, M.V., 2019. Vegetable plaiting materials from the Site of Abu Tbeirah (Southern Iraq, third millennium BC): experimental approach. *EXARC Journal* **2019/1**. <https://exarc.net/ark:/88735/10399>.
- Morozova, G., 2005. A review of Holocene avulsions of the Tigris and Euphrates rivers and possible effects on the evolution of civilizations in lower Mesopotamia. *Geoarchaeology* **20**, 401–423.
- Navabpour, P., Barrier, E., 2012. Stress states in the Zagros fold-and-thrust belt from passive margin to collisional tectonic setting. *Tectonophysics* **581**, 76–83.
- Nehme, C., Verheyden, S., Breitenbach, S. F., Gillikin, D. P., Verheyden, A., Cheng, H., Sahy, D., 2018. Climate dynamics during the penultimate glacial period recorded in a speleothem from Kanaan Cave, Lebanon (central Levant). *Quaternary Research* **90**, 10–25.
- Oliari, C., Bhattacharya, J.P., 2006. Terminal distributary channels and delta front architecture of river-dominated delta systems. *Journal of Sedimentary Research* **76**, 212–233.
- Pennington, B.T., Bunbury, J., Hovius, N., 2016. Emergence of civilization, changes in fluvio-deltaic style, and nutrient redistribution forced by Holocene sea-level rise. *Geoarchaeology* **31**, 194–210.
- Pirouz, M., Simpson, G., Chiaradia, M., 2015. Constraint on foreland basin migration in the Zagros Mountain belt using Sr isotope stratigraphy. *Basin Research* **27**, 714–728.
- Pirouz, M., Avouac, J.-P., Gualandi, A., Hassanzadeh, J., Sternai, P., 2017. Flexural bending of the Zagros foreland basin. *Geophysical Journal International* **210**, 1659–1680.
- Plaziat, J.-C., Younis, W.R., 2005. The modern environments of molluscs in southern Mesopotamia, Iraq: a guide to palaeogeographical reconstructions of Quaternary fluvial, palustrine and marine deposits. *Carnets de Géologie/Notebooks on Geology, Brest*, Article 2005/01. <https://doi.org/10.4267/2042/1453>.
- Pournelle, J., 2007. Klm to Corona: a bird's-eye view of cultural ecology and early Mesopotamian civilization. In: Stone, E.C. (Ed.), *Settlement and Society: Essays dedicated to Robert McCormick Adams*. UCLA Cotson Institute of Archaeology and Oriental Institute, Los Angeles and Chicago.
- Pournelle, J.R., 2003. *Marshland of Cities: Deltaic Landscapes and the Evolution of Early Mesopotamian Civilization*. Ph.D. thesis, Department of Anthropology, University of California, San Diego, CA.
- Pournelle, J.R., Al-Sudani, K. J., Albadran, B.N., 2019. Geoarchaeological history of the oldest site Hareer's Tells, in Basrah City, southern Iraq. *Basrah Journal of Science* **37**, 44–61.
- Reimer, P.J., Austin, W.E.N., Bard, E., Bayliss, A., Blackwell, P.G., Bronk Ramsey, C., Butzin, M., et al., 2020. The IntCal20 Northern Hemisphere Radiocarbon Age Calibration Curve (0–55 cal kBP). *Radiocarbon* **62**, 725–757.
- Romano, L., Celant, A., Montorfani, M.V. 2021. Reed-swamps in the Sumerian material culture: archaeological, archaeobotanical, experimental and epigraphic insights from the Abu Tbeirah excavations. In: Jawad, L.A. (Ed.), *Southern Iraq's Marshes: Their Environment and Conservation*. Coastal Research Library 36, Springer, Cham. https://doi-org.libproxy.viko.lt/10.1007/978-3-030-66238-7_3.
- Rost, S., Hamdani, A., George, S. 2011. Traditional dam construction in modern Iraq: a possible analogy for ancient Mesopotamian irrigation practices. *Iraq* **73**, 201–220.
- Sanlaville, P., 1989. Considérations sur l'évolution de la Basse Mésopotamie au cours des derniers millénaires. *Paléorient* **15**, 5–27.
- Sanlaville, P., 2003. The deltaic complex of the lower Mesopotamian plain and its evolution through millennia. In: Nicholson, E., Clark, P. (Eds.), *The Iraqi Marshlands*. Politico's Publishing, London, pp. 133–150.
- Schrakamp, I., 2018. Irrigation in 3rd millennium Southern Mesopotamia: cuneiform evidence from the Early Dynastic IIIb City-State of Lagash (2475–2315 BC). In: Berking J. (Ed.), *Water Management in Ancient Civilization*. Berlin, Edition Topoi, pp. 117–195.
- Sharifi, A., Pourmand, A., Canuel, E.A., Ferer-Tyler, E., Peterson, L.C., Aichner, B., Lahijani, H.A., 2015. Abrupt climate variability since the last deglaciation based on a high-resolution, multi-proxy peat record from NW Iran: the hand that rocked the cradle of civilization? *Quaternary Science Reviews* **123**, 215–230.
- Sissakian, V.K., 2000. *Geological Map of Iraq, scale 1: 1000 000*, 3rd ed. GEOSURV, Baghdad, Iraq.
- Sissakian, V.K., 2013. Geological evolution of the Iraqi Mesopotamia Foredeep, inner platform and near surroundings of the Arabian Plate. *Journal of Asian Earth Sciences* **72**, 152–163.
- Sissakian, V.K., Fouad, S.F., 2012. *Geological Map of Iraq, scale 1:1,000,000, 4th ed.* Iraq Geological Survey Publications, Baghdad, Iraq.
- Sissakian, V.K., Shihab, A.T., Al-Ansari, N., Knutsson, S., 2014. Al-Batin Alluvial Fan, southern Iraq. *Engineering* **6**, 699–711.

- Sissakian, V.K., Abdul Ahadb, A.D., Al-Ansari, N., Knutsson, S., 2018. Neotectonic activity from the upper reaches of the Arabian Gulf and possibilities of new oil fields. *Geotectonics* **52**, 240–250.
- Sissakian, V. K., Al-Ansari, N., Adamo, N., Zaiani, M. T., Abdullah, M., Laue, J. 2020. Tectonics and neotectonics of the Mesopotamian Plain: a critical review. *Journal of Earth Sciences and Geotechnical Engineering* **10**, 57–86.
- Soyer, R., 1961. Contribution à la malacologie de la Mésopotamie (Irak). *Cahiers des Naturalistes, Paris, n.s.* **17**, 65–68.
- Steinkeller, P. 2001. New light on the hydrology and topography of southern Babylonia in the third millennium. *Zeitschrift Für Assyriologie* **91**, 22–84.
- Stuiver, M., Reimer, P.J., 1993. Extended ¹⁴C data base and revised CALIB 3.0 ¹⁴C age calibration program. *Radiocarbon* **35**, 215–230.
- Tamburrino, A., 2010. Water technology in ancient Mesopotamia. In: Mays, L.W. (Ed.), *Ancient Water Technologies*. Springer, Dordrecht, Germany, pp. 29–51.
- Van Toorenburg, K.A., Donselaar, M.E., Weltje, G.J., 2018 The life cycle of crevasse splays as a key mechanism in the aggradation of alluvial ridges and river avulsion. *Earth Surface Processes and Landforms* **43**, 2409–2420.
- Verhoeven, K., 1998. *Geomorphological Research in the Mesopotamian Flood Plain*. In: *Changing Watercourses in Babylonia: Towards a Reconstruction of the Ancient Environment in Lower Mesopotamia, vol. 1*. Chicago, Oriental Institute of the University of Chicago, pp. 159–240.
- Weiss, H., Courty, M.A., Wetterstrom, W., Guichard, F., Senior, L., Meadow, R., Curnow, A., 1993. The genesis and collapse of third millennium North Mesopotamian civilization. *Science* **261**, 995–1004.
- Wilkinson, T.J., 2001. Comments on: Initial social complexity in Southwest Asia: the Mesopotamian advantage, by Guillermo Algaze. *Current Anthropology* **44**, 224–225.
- Wilkinson, T.J., Rayne, L., Jothery, J., 2015. Hydraulic landscapes in Mesopotamia: the role of human niche construction. *Water History* **7**, 397–418.
- Woolley, L., 1962. *Ur Excavations volume IX. The Neo-Babylonian and Persian Periods*. Charles Skilton Ltd., British Museum, London, 138 pp.
- Yacoub, S.Y., 2011. Stratigraphy of the Mesopotamia Plain. *Iraqi Bulletin of Geology and Mining* **4**, 47–82.
- Yacoub, S.Y., Roffa, S.H., Tawfiq, J.M., 1985. *The geology Al-Amara - Al-Nasiriya - Al-Basrah Area*. GEOSURV, internal report no. 1386, Baghdad, 247 pp.
- Yuill, B.T., Khadka, A.K., Pereira, J., Allison, M.A., Meselhe, E.A., 2016. Morphodynamics of the erosional phase of crevasse-splay evolution and implications for river sediment diversion function. *Geomorphology* **259**, 12–29.